NASA
Technical
Paper
2343

October 1984

NASA-TP-2343 19840026702

Mixed Models and Reduction Techniques for Large-Rotation, Nonlinear Analysis of Shells of Revolution With Application to Tires

Ahmed K. Noor,
Carl M. Andersen,
and John A. Tanner

NASA

NASA Technical Paper 2343

1984

Mixed Models and Reduction Techniques for Large-Rotation, Nonlinear Analysis of Shells of Revolution With Application to Tires

Ahmed K. Noor
The George Washington University
Joint Institute for Advancement of Flight Sciences
Langley Research Center
Hampton, Virginia

Carl M. Andersen
The College of William and Mary
Williamsburg, Virginia

John A. Tanner
Langley Research Center
Hampton, Virginia

National Aeronautics and Space Administration

Scientific and Technical Information Branch

CONTENTS

SUMMARY 1

INTRODUCTION 1

MATHEMATICAL FORMULATION 2
Variational Principle 2
Configuration-Dependent Load 3
Finite-Element Discretization 4
Equivalence Between Mixed Models and Displacement Models 7
Solution of Finite-Element Equations 8

MULTIPLE-PARAMETER REDUCTION TECHNIQUES 9
Degrees-of-Freedom Reduction 9
Model-Size Reduction Through Symmetry 10

NUMERICAL RESULTS 12
Accuracy of Mixed and Displacement Models 12
Isotropic circular toroid subjected to uniform internal and external pressure loads 13
Isotropic spherical cap subjected to concentrated load at the apex 13
Laminated anisotropic elliptical toroid subjected to combined internal pressure and ring loads 14
Accuracy of Degrees-of-Freedom Reduction Technique 15
Accuracy of Model Size Reduction Technique 15

DISCUSSION OF COMPUTATIONAL STRATEGY 16

CONCLUDING REMARKS 17

APPENDIX A - FUNDAMENTAL EQUATIONS OF THE NONLINEAR THEORY OF SHELLS OF REVOLUTION 19

APPENDIX B - FORMULAS FOR COEFFICIENTS IN THE FINITE-ELEMENT EQUATIONS FOR INDIVIDUAL ELEMENTS 21

APPENDIX C - EVALUATION OF PATH DERIVATIVES 25

APPENDIX D - FORM OF THE REDUCED EQUATIONS 30

REFERENCES 32

SYMBOLS 34

TABLE 39

FIGURES 40

SUMMARY

An effective computational strategy is presented for the large-rotation, nonlinear, axisymmetric analysis of shells of revolution. A total Lagrangian description of the shell deformation is used, and the analytical formulation is based on a form of Reissner's large-deformation theory including the effects of transverse shear deformation, laminated orthotropic material response, and moments acting about the normal to the middle surface. Only axisymmetric deformations are considered, and the fundamental unknowns consist of six stress resultants and three generalized displacements of the shell. The element characteristic arrays are obtained by using the Hellinger-Reissner mixed variational principle. The polynomial interpolation (or shape) functions used for approximating the stress resultants are of lower degree than those used for approximating the generalized displacements.

The three key components of the proposed computational strategy are as follows: (1) use of mixed finite-element models with discontinuous stress resultants at the element interfaces, thereby allowing the elimination of these stress resultants on the element level; (2) substantial reduction in the total number of degrees of freedom through the use of a multiple-parameter reduction technique based on perturbation expansion; and (3) reduction in the size of the analysis model through the decomposition of asymmetric loads into symmetric and antisymmetric components coupled with the use of the multiple-parameter reduction technique.

The potential of the proposed computational strategy is discussed. Numerical results are presented to demonstrate the high accuracy of the mixed models developed and to show the effectiveness of using the proposed computational strategy with these models.

INTRODUCTION

In recent years nonlinear analysis of static and dynamic problems has become the focus of intense research efforts. The increasing importance of nonlinear analysis is largely due to the emphasis placed by manufacturers, contractors, and certifying agencies on realistic modeling and accurate analysis of critical structural components. This analysis endeavor has prompted the development of versatile and powerful finite-element discretization methods as well as development of improved numerical methods and programming techniques for nonlinear analysis of structures. As this nonlinear analysis technology becomes more sophisticated, it can be used for predicting the response of a wider class of structures. One of the challenging nonlinear problems is that of predicting the response of aircraft tires during ground handling operations. The tires must be able to taxi for long distances under heavy loadings, to operate at speeds greater than 200 knots, to absorb much of the energy of the landing impacts, and to provide steering and braking forces for safe ground handling operations. Yet these tires must be as lightweight and durable as possible. To date, only a few analytical tools are available to assist the tire designer, and current design technology of tires is based largely on empirical methods. A summary of past and current modeling techniques for tires is presented in reference 1.

In addition to the diverse and severe loading conditions to which aircraft tires are subjected, several other factors contribute to the difficulty of constructing

analytical models of tires. The tire is a composite structure composed of rubber-textile constituents which exhibit anisotropic, nonhomogeneous material properties. The ground handling operations routinely result in very large rotations and large deformations in the tire. Also, the tire carcass is thick enough to allow significant transverse shear deformation to occur. All these attributes work in concert to make the development of practical analytical tire design tools extremely difficult. A shell finite-element model incorporating the effects of large rotations, laminated anisotropic material response, and transverse shear deformations, however, shows promise for tire modeling applications.

The present study constitutes a first step towards the development of computational models for tires. The objectives of this paper are twofold: (1) to present an accurate and efficient computational strategy for the nonlinear, axisymmetric analysis of shells of revolution, and (2) to demonstrate the effectiveness of the proposed strategy by means of numerical examples. The three key components of the proposed computational strategy are as follows: (1) use of mixed finite-element models with discontinuous stress resultants at the element interfaces; (2) substantial reduction in the total number of degrees of freedom through the use of a multiple-parameter reduction technique based on perturbation expansion; and (3) reduction in the size of the analysis model for symmetric structures through the decomposition of asymmetric loadings into symmetric and antisymmetric components coupled with the use of the multiple-parameter reduction technique. To sharpen the focus of the present study, axisymmetric static and large-rotation problems of shells of revolution are considered. A total Lagrangian description of the shell deformation is used, and the analytical formulation is based on a form of Reissner's large-deformation theory with the effects of transverse shear deformation, laminated orthotropic material response, and moments acting around the normal to the middle surface included. The mixed models presented herein have both stress resultants and generalized displacements as fundamental unknowns. The stress resultants are allowed to be discontinuous at interelement boundaries.

MATHEMATICAL FORMULATION

Variational Principle

The analytical formulation is based on a form of Reissner's large-deformation theory of shells of revolution (see ref. 2 and appendix A) with the effects of transverse shear deformation, laminated orthotropic material response, and moments acting around the normal to the middle surface included. Only axisymmetric deformations of the shell are considered, and the load can be displacement dependent as well as nonconservative. The load is represented by two independent parameters $q^{(1)}$ and $q^{(2)}$ A mixed formulation is used in which the fundamental unknowns consist of the stress resultants N_s, N_θ, M_s, M_θ, Q_s, and M_n and the generalized displacements of the middle surface u, w, and ϕ. (See fig. 1 for sign convention.) A total Lagrangian description of the shell deformation is used, and the shell configurations at different load levels are referred to the initial coordinate system of the undeformed shell.

The mixed variational principle used in the element development is given by

$$\delta\Pi(N_s,N_\theta,M_s,M_\theta,Q_s,M_n,u,w,\phi) = \delta\bar{\Pi} - \delta W = 0 \tag{1}$$

where

$$\bar{\Pi} = \int \Big\{ N_s \left[\cos(\phi + \phi_o)\ \partial u - \sin(\phi + \phi_o)\ \partial w + \cos\phi - 1\right] + N_\theta \left(\frac{u}{r}\right) + M_s\ \partial\phi + M_\theta \left[\sin(\phi + \phi_o) - \sin\phi_o\right]/r + Q_s \left[\sin(\phi + \phi_o)\ \partial u + \cos(\phi + \phi_o)\ \partial w + \sin\phi\right] + M_n \left[\cos(\phi + \phi_o) - \cos\phi_o\right]/r - \Big[\frac{1}{2}\left(a_{11} N_s^2 + a_{22} N_\theta^2 + g_{11} M_s^2 + g_{22} M_\theta^2 + a_s Q_s^2 + g_n M_n^2\right) + a_{12} N_s N_\theta + b_{11} N_s M_s + b_{12} N_s M_\theta + b_{12} N_\theta M_s + b_{22} N_\theta M_\theta + g_{12} M_s M_\theta\Big] \Big\} 2\pi r\ ds \qquad (2)$$

and

$$\delta W = \int (p_u\ \delta u + p_w\ \delta w + m\ \delta\phi)\ 2\pi r\ ds + \Sigma\ (\tilde{P}_u\ \delta u + \tilde{P}_w\ \delta w + \tilde{M}\ \delta\phi) - \Sigma\ (\delta P_u\ \tilde{u} + \delta P_w\ \tilde{w} + \delta M\ \tilde{\phi}) \qquad (3)$$

In equations (2) and (3), the quantity ϕ_o is the angle between the axis of revolution and a normal to the undeformed middle surface; ϕ is the rotation of the shell middle surface; r is the radius of the undeformed parallel circle; a, b, and g are shell compliance coefficients (inverses of shell stiffnesses; see appendix A); p_u and p_w are the intensities of external distributed loads in the radial and axial directions; m is the intensity of external distributed meridional moment; P_u, P_w, and M are the external concentrated loads and meridional moment (or total values of ring loads and moments); and $\partial \equiv \frac{d}{ds}$. The quantities in equation (3) with a tilde (~) denote prescribed forces and displacements. The summation sign in equation (3) extends over all applied external forces and prescribed displacements in the shell meridian.

Configuration-Dependent Load

For the case of uniform hydrostatic pressure, the direction of the load always remains perpendicular to the deformed middle surface of the shell; thus, the load is

configuration dependent. In this case, the expressions for the external load components are given by

$$p_u = p_o(1 + \varepsilon_{so}) \left(1 + \frac{u}{r}\right) \sin(\phi + \phi_o - \gamma_o) \tag{4}$$

$$p_w = p_o(1 + \varepsilon_{so}) \left(1 + \frac{u}{r}\right) \cos(\phi + \phi_o - \gamma_o) \tag{5}$$

$$m = 0 \tag{6}$$

where p_o is the pressure load (per unit area of the deformed middle surface); ε_{so} is the extensional strain in the meridional direction; and γ_o is the transverse shearing strain. (See appendix A.)

Finite-Element Discretization

The finite-element discretization is performed by dividing the shell meridian into finite elements. The generalized displacements u, w, and ϕ are approximated by sums of products of shape functions N and of nodal displacements X_i. The stress resultants N_s, N_θ, M_s, M_θ, Q_s, and M_n are approximated by sums of products of shape functions $\bar{N}$ and stress-resultant parameters H_J.

The governing finite-element equations for each individual element are obtained by first replacing the generalized displacements and stress resultants with their expressions in terms of the shape functions and then applying the variational principle (eqs. (1) to (3)). If the nodal displacements X_j and stress-resultant parameters H_J are varied independently and simultaneously, one obtains the following set of equations for each element:

$$\bar{f}_I \equiv -F_{IJ} H_J + S_{Ij} X_j + \sum_\alpha \left[\left(A_I^{(\alpha)} + B_{Ij}^{(\alpha)} X_j\right) \cos \phi^{(\alpha)} + \left(\bar{A}_I^{(\alpha)} + \bar{B}_{Ij}^{(\alpha)} X_j\right) \sin \phi^{(\alpha)}\right] - R_I = 0 \tag{7}$$

$$f_i \equiv S_{Ji} H_J + \sum_\alpha \left\{\left[B_{Ji}^{(\alpha)} + T_i^{(\alpha)} \left(\bar{A}_J^{(\alpha)} + \bar{B}_{J\ell}^{(\alpha)} X_\ell\right)\right] H_J \cos \phi^{(\alpha)} + \left[\bar{B}_{Ji}^{(\alpha)} - T_i^{(\alpha)} \left(A_J^{(\alpha)} + B_{J\ell}^{(\alpha)} X_\ell\right)\right] H_J \sin \phi^{(\alpha)}\right\} - q^{(1)} \left(P_i^{(1)} + Q_{ij}^{(1)} X_j\right) - q^{(2)} \left(P_i^{(2)} + Q_{ij}^{(2)} X_j\right) = 0 \tag{8}$$

where the array $T_i^{(\alpha)}$ is defined by the following equation:

$$\phi^{(\alpha)} = T_i^{(\alpha)} X_i \tag{9}$$

The F and S terms are the linear flexibility and strain-displacement coefficients; $P^{(1)}$ and $P^{(2)}$ are normalized consistent-load coefficients; $Q^{(1)}$ and $Q^{(2)}$ are normalized load stiffness coefficients, which are symmetric for conservative loadings and asymmetric for nonconservative loadings; $q^{(1)}$ and $q^{(2)}$ are load parameters; A, B, $\bar{A}$, and $\bar{B}$ are multipliers of the trigonometric contributions; R_I are integrals of shape functions $\left(\text{which cancel with the } A_I^{(\alpha)} \text{ terms when } \phi^{(\alpha)} = 0\right)$; and superscript α denotes that the quantity is evaluated at the numerical quadrature point. The summation sign extends over the n numerical quadrature points in the element. The range of the lowercase indices is 1 to 3m (where m is the number of displacement nodes), and the range of the uppercase indices is 1 to 6δ (where δ is the number of nodes or parameters used in approximating each of the stress resultants within the individual elements); a repeated subscript in the same term denotes summation over its full range. The explicit forms of the arrays F, S, A, B, $\bar{A}$, $\bar{B}$, R, T, $P^{(1)}$, $P^{(2)}$, $Q^{(1)}$, and $Q^{(2)}$ are given in appendix B.

Note that in equation (8) the two loads $P_i + Q_{ij}X_j$ are assumed to be linear functions of the nodal displacements X_j (which is a reasonable approximation for the case of uniform hydrostatic pressure in eqs. (4) to (6)). The validity of this approximation is discussed in the section entitled "Numerical Results." Other displacement-dependent and nonconservative loads are discussed in reference 3.

The continuity of the stress resultants N_s, N_θ, M_s, M_θ, Q_s, and M_n is not imposed at interelement boundaries. Therefore, the stress-resultant parameters H_J can be eliminated on the element level from equations (7) and (8), and one obtains the following elemental equations in the nodal displacements X_j:

$$\begin{aligned}
&K_{ij} X_j + \sum_\alpha \Big[\left(A_i^{(\alpha)} + B_{ij}^{(\alpha)} X_j + C_{ijk}^{(\alpha)} X_j X_k\right) \cos \phi^{(\alpha)} \\
&\quad + \left(\bar{A}_i^{(\alpha)} + \bar{B}_{ij}^{(\alpha)} X_j + \bar{C}_{ijk}^{(\alpha)} X_j X_k\right) \sin \phi^{(\alpha)}\Big] \\
&\quad + \sum_\alpha \sum_\beta \Big[\left(D_i^{(\alpha,\beta)} + E_{ij}^{(\alpha,\beta)} X_j + F_{ijk}^{(\alpha,\beta)} X_j X_k\right) \cos \phi^{(\alpha)} \cos \phi^{(\beta)} \\
&\quad + \left(\bar{D}_i^{(\alpha,\beta)} + \bar{E}_{ij}^{(\alpha,\beta)} X_j + \bar{F}_{ijk}^{(\alpha,\beta)} X_j X_k\right) \sin \phi^{(\alpha)} \sin \phi^{(\beta)} \\
&\quad + \left(\tilde{D}_i^{(\alpha,\beta)} + \tilde{E}_{ij}^{(\alpha,\beta)} X_j + \tilde{F}_{ijk}^{(\alpha,\beta)} X_j X_k\right) \cos \phi^{(\alpha)} \sin \phi^{(\beta)}\Big] \\
&\quad - R_i - q^{(1)} \left(P_i^{(1)} + Q_{ij}^{(1)} X_j\right) - q^{(2)} \left(P_i^{(2)} + Q_{ij}^{(2)} X_j\right) = 0
\end{aligned} \tag{10}$$

where

$$\mathcal{K}_{ij} = S_{Ii}\ (F^{-1})_{IJ}\ S_{Jj} \tag{11}$$

$$\mathcal{A}_i^{(\alpha)} = S_{Ii}\ (F^{-1})_{IJ}\ A_J^{(\alpha)} - \underline{\left(B_{Ii}^{(\alpha)} + T_i^{(\alpha)}\ \bar{A}_I^{(\alpha)}\right)\ (F^{-1})_{IJ}}\ R_J \tag{12}$$

$$\mathcal{B}_{ij}^{(\alpha)} = S_{Ii}\ (F^{-1})_{IJ}\ B_{Jj}^{(\alpha)} + \underline{\left(B_{Ii}^{(\alpha)} + T_i^{(\alpha)}\ \bar{A}_I^{(\alpha)}\right)\ (F^{-1})_{IJ}}\ S_{Jj} - \underline{T_i^{(\alpha)}\ \bar{B}_{Ij}^{(\alpha)}\ (F^{-1})_{IJ}}\ R_J \tag{13}$$

$$\mathcal{C}_{ijk}^{(\alpha)} = \underline{T_i^{(\alpha)}\ \bar{B}_{Ij}^{(\alpha)}\ (F^{-1})_{IJ}}\ S_{Jk} \tag{14}$$

$$\mathcal{D}_i^{(\alpha,\beta)} = \underline{\left(B_{Ii}^{(\alpha)} + T_i^{(\alpha)}\ \bar{A}_I^{(\alpha)}\right)\ (F^{-1})_{IJ}}\ A_J^{(\beta)} \tag{15}$$

$$\mathcal{E}_{ij}^{(\alpha,\beta)} = \underline{T_i^{(\alpha)}\ \bar{B}_{Ij}^{(\alpha)}\ (F^{-1})_{IJ}}\ A_J^{(\beta)} + \underline{\left(B_{Ii}^{(\alpha)} + T_i^{(\alpha)}\ \bar{A}_I^{(\alpha)}\right)\ (F^{-1})_{IJ}}\ B_{Jj}^{(\beta)} \tag{16}$$

$$\mathcal{F}_{ijk}^{(\alpha,\beta)} = \underline{T_i^{(\alpha)}\ \bar{B}_{Ij}^{(\alpha)}\ (F^{-1})_{IJ}}\ B_{Jk}^{(\beta)} \tag{17}$$

$$\tilde{\mathcal{D}}_i^{(\alpha,\beta)} = \underline{\left(B_{Ii}^{(\alpha)} + T_i^{(\alpha)}\ \bar{A}_I^{(\alpha)}\right)\ (F^{-1})_{IJ}}\ \bar{A}_J^{(\beta)} + \underline{\left(\bar{B}_{Ii}^{(\beta)} - T_i^{(\beta)}\ A_I^{(\beta)}\right)\ (F^{-1})_{IJ}}\ A_J^{(\alpha)} \tag{18}$$

$$\tilde{\mathcal{E}}_{ij}^{(\alpha,\beta)} = \underline{\left(B_{Ii}^{(\alpha)} + T_i^{(\alpha)}\ \bar{A}_I^{(\alpha)}\right)\ (F^{-1})_{IJ}}\ \bar{B}_{Jj}^{(\beta)} + \underline{T_i^{(\alpha)}\ \bar{B}_{Ij}^{(\alpha)}\ (F^{-1})_{IJ}}\ \bar{A}_J^{(\beta)}$$

$$+ \underline{\left(\bar{B}_{Ii}^{(\beta)} - T_i^{(\beta)}\ A_I^{(\beta)}\right)\ (F^{-1})_{IJ}}\ B_{Jj}^{(\alpha)} - T_i^{(\beta)}\ B_{Ij}^{(\beta)}\ (F^{-1})_{IJ}\ A_J^{(\alpha)} \tag{19}$$

$$\tilde{\mathcal{F}}_{ijk}^{(\alpha,\beta)} = \underline{T_i^{(\alpha)}\ \bar{B}_{Ij}^{(\alpha)}\ (F^{-1})_{IJ}}\ \bar{B}_{Jk}^{(\beta)} - T_i^{(\beta)}\ B_{Ij}^{(\beta)}\ (F^{-1})_{IJ}\ B_{Jk}^{(\alpha)} \tag{20}$$

$$\mathcal{R}_i = S_{Ii}\ (F^{-1})_{IJ}\ R_J \tag{21}$$

The arrays $\bar{\mathcal{A}}$, $\bar{\mathcal{B}}$, $\bar{\mathcal{C}}$, $\bar{\mathcal{D}}$, $\bar{\mathcal{E}}$, and $\bar{\mathcal{F}}$ are obtained from the definitions of the corresponding arrays $\mathcal{A}$, $\mathcal{B}$, $\mathcal{C}$, $\mathcal{D}$, $\mathcal{E}$, and $\mathcal{F}$ by replacing the respective arrays A, B, $\bar{A}$, $\bar{B}$, and T in equations (12) to (21) with $\bar{A}$, $\bar{B}$, A, B, and -T. Sub-

expressions which occur repeatedly in equations (11) to (21) are underlined with dashed, dotted, or dashed-dotted lines as appropriate. The linear finite-element equations for an individual element can be obtained from equation (10) by setting

$$\sin \phi^{(\alpha)} = \phi^{(\alpha)} = T_j^{(\alpha)} X_j$$

$$\cos \phi^{(\alpha)} = 1$$

and neglecting the nonlinear terms. The resulting equations can be cast in the following form:

$$\left(\overset{*}{K}_{ij} - q^{(1)} \, Q_{ij}^{(1)} - q^{(2)} \, Q_{ij}^{(2)}\right) X_j = q^{(1)} \, P_i^{(1)} + q^{(2)} \, P_i^{(2)} \tag{22}$$

where $\overset{*}{K}_{ij}$ are the linear stiffness coefficients (excluding the load stiffness contributions Q_{ij}) for individual elements given by

$$\overset{*}{K}_{ij} = K_{ij} + \sum_{\alpha} \left(B_{ij}^{(\alpha)} + \bar{A}_i^{(\alpha)} \, T_j^{(\alpha)}\right) + \sum_{\alpha} \sum_{\beta} \left(E_{ij}^{(\alpha,\beta)} + \tilde{D}_i^{(\alpha,\beta)} \, T_j^{(\beta)}\right) \tag{23}$$

The R_i terms are absent in the linear equation (22) because they cancel out the combination of $\sum_{\alpha} A_i^{(\alpha)}$ and $\sum_{\alpha} \sum_{\beta} D_i^{(\alpha,\beta)}$.

Equivalence Between Mixed Models and Displacement Models

A fixed model with discontinuous stress resultants at interelement boundaries is said to be *equivalent* to a displacement model if, after elimination of the stress-resultant parameters (on the element level), the resulting finite-element equations for the two models are *identical* (i.e., eq. (10) for the mixed model is identical to the corresponding equation for the displacement model). The models are said to be *nearly equivalent* if their finite-element equations are *almost identical* (e.g., if the corresponding numerical coefficients in both sets of equations differ by a small percentage).

The equivalence between mixed models and some classes of displacement models was first established in reference 4 for linear problems. It was extended to moderate-rotation nonlinear problems of curved beams and shallow shells in references 5 and 6.

For axisymmetric, large-rotation, nonlinear problems of shells of revolution with constant material properties, the following two groups of equivalent mixed and displacement models can be identified:

Group 1 - Equivalent mixed models and standard displacement models. The conditions for the equivalence are as follows:

1. The same number of nodes m and Lagrangian interpolation functions are used for approximating the generalized displacements u, w, and ϕ in both the displacement and mixed models.

2. The number of quadrature points n in the Gauss-Legendre quadrature formula used for the numerical evaluation of all terms of the mixed and displacement models is equal to the number of displacement nodes.

3. The polynomial interpolation functions for the stress resultants N_s, N_θ, M_s, M_θ, Q_s, and M_n in the mixed models are of the same degree as those of displacements and the stress resultants are allowed to be discontinuous at interelement boundaries.

Group 2 - Equivalent mixed models and reduced integration displacement models. The conditions for the equivalence are as follows:

1. The same number of nodes m and Lagrangian interpolation functions are used for approximating the generalized displacements u, w, and ϕ in both the displacement and mixed models.

2. The same low-order Gauss-Legendre quadrature formula (i.e., $n < m$) is used for the numerical evaluation of all integrals in the displacement and mixed models.

3. The interpolation functions for the stress resultants N_s, N_θ, M_s, M_θ, Q_s, and M_n in the mixed models are polynomials of lower degree than those of the displacement models, and the stress resultants are allowed to be discontinuous at interelement boundaries. The number of stress-resultant interpolation functions δ equals the number of quadrature points per element n. Of particular interest is the case where $n = \delta = m - 1$ (where m is the number of displacement nodes), and thus the interpolation functions for the stress resultants are polynomials one degree lower than those of displacements.

Henceforth, the mixed and displacement models of group 1 are designated by MDm-m and DEm. The corresponding models of group 2 are designated by MDm-n and DRm-n. The aforementioned equivalences are based on comparing the *exact analytic expressions for the stiffness coefficients* of the mixed and displacement models. Numerical experiments have demonstrated the superior performance of the models of group 2 over those of group 1. This result is demonstrated in the "Numerical Results" section.

Solution of Finite-Element Equations

The assembled finite-element equations (obtained from eqs. (7) and (8)) for the shell can be represented in the following compact form:

$$\begin{Bmatrix} \bar{f}_{\bar{H}} \\ \bar{f}_{\bar{X}} \end{Bmatrix} = \begin{bmatrix} -\bar{\mathcal{F}} & \bar{\mathcal{S}} \\ \bar{\mathcal{S}}^t & 0 \end{bmatrix} \begin{Bmatrix} \bar{H} \\ \bar{X} \end{Bmatrix} + \begin{Bmatrix} \bar{\mathcal{G}}(\bar{X}) \\ \bar{\mathcal{M}}(\bar{H},\bar{X}) \end{Bmatrix} - \begin{Bmatrix} \bar{\mathcal{R}} \\ 0 \end{Bmatrix} - q^{(1)} \begin{Bmatrix} 0 \\ \bar{\mathcal{Q}}^{(1)}(\bar{X}) \end{Bmatrix} - q^{(2)} \begin{Bmatrix} 0 \\ \bar{\mathcal{Q}}^{(2)}(\bar{X}) \end{Bmatrix} = 0 \qquad (24)$$

where $[\bar{\mathcal{F}}]$ is a block diagonal matrix containing the elemental contributions F_{IJ}; $[\bar{\mathcal{S}}]$ is a rectangular matrix containing the S_{Ij} contributions; $\{\bar{\mathcal{G}}(\bar{X})\}$ and $\{\bar{\mathcal{M}}(\bar{H},\bar{X})\}$ are the vectors of trigonometric contributions; $\{\bar{X}\}$ is the assembled vector of nodal displacements; $\{\bar{H}\}$ is the assembled vector of stress-resultant parameters; $\{\bar{\mathcal{R}}\} = \{\bar{\mathcal{G}}(0)\}$ is a constant vector composed of the elemental contributions R_I; $\{\bar{\mathcal{Q}}^{(1)}(\bar{X})\}$ and $\{\bar{\mathcal{Q}}^{(2)}(\bar{X})\}$ are the vectors of normalized external forces; and superscript t denotes transposition. Note that the linear global generalized stiffness matrix is given by

$$\begin{bmatrix} -\bar{\mathcal{F}} & \bar{\mathcal{S}} \\ \text{Symm.} & 0 \end{bmatrix} + \begin{bmatrix} 0 & \dfrac{\partial \bar{\mathcal{G}}_{\bar{I}}}{\partial \bar{X}_{\bar{j}}} \\ \text{Symm.} & \dfrac{\partial \bar{\mathcal{M}}_{\bar{i}}}{\partial \bar{X}_{\bar{j}}} \end{bmatrix}_{q^{(1)}=q^{(2)}=0} \tag{25}$$

where $\bar{I}$ ranges from 1 to $6\bar{\delta}$ (total number of stress-resultant parameters in the discretized shell); and $\bar{i}$ and $\bar{j}$ range from 1 to $3\bar{m}$ (total number of displacement nodes in the discretized shell).

The solution of equation (24) is usually carried out by using an incremental-iterative technique (i.e., a predictor-corrector continuation method) wherein the vectors $\{\bar{H}\}$ and $\{\bar{X}\}$ corresponding to a particular pair of values of the load parameters $q^{(1)}$ and $q^{(2)}$ are used to calculate suitable approximations (predictors) for $\{\bar{H}\}$ and $\{\bar{X}\}$ at different values of $q^{(1)}$ and $q^{(2)}$. These approximations are then chosen as initial estimates for $\{\bar{H}\}$ and $\{\bar{X}\}$ in a corrective-iterative scheme such as the Newton-Raphson technique.

MULTIPLE-PARAMETER REDUCTION TECHNIQUES

Degrees-of-Freedom Reduction

In recent years considerable progress has been made in the development of techniques for reducing the total number of degrees of freedom of the discretized structure without sacrificing the accuracy of predicting the nonlinear response. Such techniques are called reduction methods and are essentially hybrid procedures combining the finite-element method with the classic Rayleigh-Ritz technique. (See refs. 7, 8, and 9.) The effectiveness of reduction methods for the nonlinear and postbuckling analyses of structures subjected to multiple independent loads has been demonstrated in references 10 and 11. A possible approach for applying multiple-parameter reduction methods in conjunction with the mixed formulation for the large-rotation, nonlinear analysis of shells of revolution is to use finite elements for the initial discretization of the shell and to express the vectors of unknown stress resultants $\{\bar{H}\}$ and generalized displacements $\{\bar{X}\}$ as a linear combination of a small number of global approximation (or basis) vectors. A Rayleigh-Ritz (or Bubnov-Galerkin) technique is then used to approximate the finite-element equations by a reduced system of nonlinear equations. This approach was applied to nonlinear large-rotation problems of curved beams in reference 12.

An effective choice for the basis vectors consists of a solution of the nonlinear finite-element equations (eqs. (24)) and its various-order path derivatives. Both the solution and the path derivatives are obtained at a particular pair of values $q^{(1)}$ and $q^{(2)}$. For the case of two independent load parameters $q^{(1)}$ and $q^{(2)}$, the path derivatives are given by

$$\left.\begin{aligned} \{\bar{H}\} &= [\bar{\Gamma}]\ \{\psi\} \\ \{\bar{X}\} &= [\Gamma]\ \{\psi\} \end{aligned}\right\} \tag{26}$$

where

$$[\bar{\Gamma}] = \left[\{\bar{H}\} \left\{\frac{\partial \bar{H}}{\partial \lambda_1}\right\} \left\{\frac{\partial \bar{H}}{\partial \lambda_2}\right\} \left\{\frac{\partial^2 \bar{H}}{\partial \lambda_1^2}\right\} \left\{\frac{\partial^2 \bar{H}}{\partial \lambda_1\, \partial \lambda_2}\right\} \left\{\frac{\partial^2 \bar{H}}{\partial \lambda_2^2}\right\} \cdots\right] \tag{27}$$

$$[\Gamma] = \left[\{\bar{X}\} \left\{\frac{\partial \bar{X}}{\partial \lambda_1}\right\} \left\{\frac{\partial \bar{X}}{\partial \lambda_2}\right\} \left\{\frac{\partial^2 \bar{X}}{\partial \lambda_1^2}\right\} \left\{\frac{\partial^2 \bar{X}}{\partial \lambda_1\, \partial \lambda_2}\right\} \left\{\frac{\partial^2 \bar{X}}{\partial \lambda_2^2}\right\} \cdots\right] \tag{28}$$

In equations (27) and (28), λ_1 and λ_2 are the path parameters and $\{\psi\}$ is the vector of undetermined coefficients, which are functions of λ_1 and λ_2. The number of basis vectors r is considerably smaller than the total number of degrees of freedom of the shell model. The path parameters λ_1 and λ_2 can be identified with load, displacement, or pseudo arc-length parameters. (See ref. 11.)

The equations used in evaluating the basis vectors are obtained by successive differentiation (with respect to λ_1 and λ_2) of the finite-element equations of the discretized shell (eqs. (24)). The explicit forms of the first few of these equations are given in appendix C. The path derivatives of the stress resultants can be eliminated on the element level, thereby reducing the size of the equations required for evaluating the displacement path derivatives. Note that even for the nonconservative load case, the equations used in the generation of the initial basis vectors are symmetric. (See appendix C.)

The explicit forms of the reduced system of equations in terms of the unknowns $\{\psi\}$ are given in appendix D. Note that for large-rotation problems, the form of these equations is considerably more complicated than the corresponding equations for moderate rotations. In both cases, however, the number of reduced degrees of freedom is small. The computational procedure used in conjunction with the reduction method is described in references 11 and 12 and is not repeated herein.

Model-Size Reduction Through Symmetry

It has long been recognized that the size of the analysis model of a structure can be reduced by exploiting the *a priori* known symmetries of the response of that structure. Considerable effort has been devoted to identifying symmetries exhibited by various types of structures and exploiting these symmetries in their finite-element

analysis. For linear symmetric structures subjected to asymmetric external load, symmetry concepts can be used by decomposing the load into symmetric and antisymmetric systems. It is generally assumed, however, that such a decomposition is not useful for nonlinear problems in which the principle of superposition is not applicable. In fact, the nonlinear response to an antisymmetric load is, in general, asymmetric. In this section a simple procedure is outlined for reducing the size of the model needed for the nonlinear analysis of a structure through (1) the decomposition of the asymmetric load into symmetric and antisymmetric components and (2) the use of the multiple-parameter reduction technique described in the preceding section. For convenience, the procedure is described herein for the case of a toroidal shell with a symmetric meridian (mirror symmetry in a plane normal to the axis of revolution of the toroid) subjected to asymmetric ring load (which is independent of the circumferential coordinate θ). (See fig. 2.) The meridian is assumed to be in the form of an incomplete ellipse.

The key elements of the procedure are as follows:

1. The given asymmetric ring load is decomposed into symmetric and antisymmetric systems of ring loads; that is,

$$q\,P_i = q^{(1)}\,P_i^{(1)} + q^{(2)}\,P_i^{(2)} \tag{29}$$

where q, $q^{(1)}$, and $q^{(2)}$ are normalizing load parameters; P_i are the normalized components of the given asymmetric load; and $P_i^{(1)}$ and $P_i^{(2)}$ are the normalized components of the symmetric and antisymmetric loads. (See fig. 2.)

2. The basis vectors (path derivatives with respect to $q^{(1)}$ and $q^{(2)}$) are evaluated at $q^{(1)} = q^{(2)} = 0$. *Only half the shell meridian is used in generating these vectors,* and the following symmetry (and antisymmetry) conditions are used for the generalized displacements:

$$\frac{\partial^{m+n}}{\partial\lambda_1^m\,\partial\lambda_2^n}\begin{Bmatrix} u(-s) \\ w(-s) \\ \phi(-s) \end{Bmatrix} = \frac{\partial^{m+n}}{\partial\lambda_1^m\,\partial\lambda_2^n}\begin{Bmatrix} (-1)^n\,u(s) \\ -(-1)^n\,w(s) \\ -(-1)^n\,\phi(s) \end{Bmatrix} \tag{30}$$

where λ_1 is in this case equal to the symmetric load parameter $q^{(1)}$ and λ_2 is equal to the antisymmetric load parameter $q^{(2)}$. Note that the symmetry conditions at the centerline are independent of m and that there are two sets of conditions corresponding to even and odd values of n.

3. The reduced equations (for the full toroidal shell) are generated and the nonlinear response is traced by marching with the reduced equations in the two-dimensional load space spanned by the load parameters $q^{(1)}$ and $q^{(2)}$. Each pair of values $\left(q^{(1)}\right.$ and $\left.q^{(2)}\right)$ is selected to correspond to a value of the given load parameter q. (See eq. (29).)

The following four comments with regard to the computational procedure are in order:

1. Although the individual basis vectors exhibit symmetry (or antisymmetry), their linear combination which approximates the solution for the original asymmetric load is generally asymmetric.

2. The reduced equations can be formed by using only half the shell meridian. However, the solution of these equations approximates the asymmetric response over the full meridian.

3. In case the given load is antisymmetric, the procedure can be simplified since only one λ is needed. Obviously, for symmetric loads, the response is symmetric.

4. Updated sets of basis vectors may be formed by using the procedure, but it is essential that the shell configuration used in generating these vectors be symmetric (e.g., $q^{(2)} = 0$).

NUMERICAL RESULTS

Accuracy of Mixed and Displacement Models

To test and evaluate the performance of the mixed models with discontinuous stress resultants developed herein, several large-rotation, nonlinear problems of shells of revolution have been solved with these models. In all the problems considered, the material is assumed to be linearly elastic. Comparisons are made with converged mixed and displacement model solutions and with previously published solutions (whenever available) to assess the accuracy and convergence of different models. The results of the following three problem sets are presented herein: (1) isotropic circular toroid subjected to uniform internal and external pressure loads; (2) isotropic spherical cap subjected to a concentrated load at the apex; and (3) laminated anisotropic elliptical toroid subjected to combined internal pressure and ring loads.

Because of the axial symmetry of the load and the shell response, only one meridian is considered and analyzed by using the following: (1) the mixed models developed herein (MDm-m and MDm-n); (2) the standard displacement model based on normal integration (DEm); and (3) the displacement models based on reduced integration (DRm-n). The characteristics of the different finite-element models are summarized in table 1. For all the problems considered the mixed models MD2-1 and MD3-2 are equivalent (in the sense described in the section entitled "Equivalence Between Mixed Models and Displacement Models") to the corresponding reduced-integration displacement models DR2-1 and DR3-2. The toroidal shells considered herein have symmetric meridians, and therefore only half the meridians of these shells are analyzed. In all three problems, an arc-length control method is used (see refs. 9 and 11) to limit the load step size and to circumvent the difficulties associated with the singularity of the stiffness matrix near critical points.

A solution based on the multisegment integration technique for the first problem is presented in reference 13. Finite-element solutions for the same problem are given in references 14 and 15. Analytic solutions for the spherical cap problem (for slightly different data) are given in reference 16. Finite-element solutions for the spherical cap problem are given in reference 17.

Isotropic circular toroid subjected to uniform internal and external pressure loads.- The first problem considered is that of an isotropic circular toroid subjected to uniform internal and external pressure loads p_o. The material and geometric characteristics of the shell and the responses of the shell to uniform internal and external pressures are shown in figure 3. Also shown are the actual deformed meridians of the shell corresponding to three different values of the external pressure p_o (designated by 1, 2, and 3). The response of the shell to external pressure exhibits limit-point behavior. After the first limit point, the displacements and strain energies of the shell are considerably larger for external pressure than for the same numerical values of internal pressure. Previous solutions to this problem were limited to the case of external pressure with magnitude of $|p_o/E| \leq 1.1 \times 10^{-5}$ (no limit point).

For all the loads considered, the transverse shear strain energy is negligible. The extensional energy is the dominant energy (more than 50 percent of the total energy) for internal pressure load and for external pressure up to the limit point. The bending energy builds up rapidly after the limit point and becomes the dominant energy at $|w_c/h| \geq 2.0$. It reaches 86 percent of the total energy at $|w_c/h| = 12.0$. For the loads considered, the predictions of the moderate-rotation Sanders-Budiansky theory (refs. 18 and 19) are almost identical to those of Reissner's large-rotation theory used in the present study. (See fig. 3.) Also, the response to displacement-dependent follower load (live load) is nearly identical to that of a constant-directional normal load.

The accuracy and convergence of the solutions obtained with the different models listed in table 1 are indicated in figures 4 and 5. The standard of comparison is taken to be the solution obtained by using 24 MD4-3 elements. Figure 4 shows the accuracy of the displacement w_c/h and the total strain energy of the shell obtained with the different displacement and mixed models. Figure 5 shows the distribution of the displacements and stress resultants obtained with the different mixed models along the shell meridian at $p_o/E = -1.1 \times 10^{-5}$. As expected, the solutions obtained by using 24 DE2 elements are far removed from the converged solution. In the load range considered, no limit point is predicted with this model. The accuracy of the solutions improves by using 12 DE3 elements. Further improvement is obtained by using eight DE4 elements (all having the same total number of degrees of freedom). On the other hand, the solutions obtained with the present mixed models are considerably more accurate than those obtained with the corresponding displacement models. For the same total number of degrees of freedom, the predictions of the MD4-3 model are more accurate than those obtained with the MD3-2 and MD2-1 models. This is particularly true in the region along the meridian where sharp variations occur in the various displacements and stress resultants. (See fig. 5.)

Isotropic spherical cap subjected to concentrated load at the apex.- The second problem considered is that of the nonlinear response of an isotropic spherical cap subjected to a concentrated load at the apex. The concentrated load retains its vertical direction throughout the deformation process. The shell properties are given in figure 6. The cap is simply supported at its boundary. The response of the shell exhibits both snap-through as well as snap-back phenomena. The transverse shear strain energy is negligible throughout the load range considered. The nonlinear responses predicted with the present large-rotation theory and the moderate-rotation Sanders-Budiansky theory are shown in figure 6. Also, the deformed configurations of the shell for five different values of concentrated load, as predicted with the large-rotation theory, are shown in figure 6. The five loads correspond to points 1 to 5 in the lower left-hand part of the figure. As can be seen in figure 6, the agreement

between the predictions of the two theories is limited to the initial phase of the response (with maximum displacements of the order of $4.0h$ and maximum rotation of the order of 30°), after which the moderate-rotation theory overestimates both the displacements and the total strain energy of the shell.

In the load range considered, the bending energy is the dominant energy. At $q = P R/E h^3 = -3.56$, the bending energy is 87.3 percent of the total strain energy. The extensional and transverse shear strain energies are only 9.7 percent and 3.0 percent of the total strain energy.

The accuracy of the maximum displacement w_c and of the total strain energy U obtained by using 12 MD2-1 elements, 6 MD3-2 elements, and 4 MD4-3 elements (all having the same total number of degrees of freedom) is indicated in figure 7. As can be seen in figure 7, only a slight improvement in accuracy (at higher loads) is obtained by using the higher order mixed models for the same total number of degrees of freedom.

Laminated anisotropic elliptical toroid subjected to combined internal pressure and ring loads.- As a final example, consider the nonlinear response of the 10-layered, anisotropic elliptical toroid shell shown in figure 8. The shell has clamped edges ($u = w = \phi = 0$) and is subjected to combined internal pressure p_o and a ring load P. The nonlinear responses predicted with the present large-rotation theory and with the moderate-rotation Sanders-Budiansky theory are shown in figure 9. To simplify the analysis, the anisotropic bending-extensional coupling coefficients of the shell laminate are neglected (i.e., the shell is treated as orthotropic). Two cases of internal pressure loads are considered. In the first case, the internal pressure has an intensity p_o per unit area of the undeformed middle surface and is assumed to remain normal to the undeformed middle surface throughout the deformation process. The second case is that of a live load of intensity p_o per unit area of the deforming middle surface, and the load remains normal to the deformed middle surface. Also, the deformed configurations of the shell corresponding to $p_o/E_L = 0.66 \times 10^{-3}$ and to three different values of the ring load P as predicted with the large-rotation theory are shown in figure 10. The three ring load values correspond to points 1, 2, and 3 in the left figure. Note that for shear deformation shell theory, the clamped boundary conditions used do not imply that $dw/ds = 0$. As can be seen in figure 9, the predictions of the moderate-rotation theory are considerably in error, particularly for higher loads. Also, the response of the shell to live loads is substantially different from the response to constant, directional loads.

The transverse shear strain energy is significant. For example, at $q^{(1)} = 0.66 \times 10^{-3}$ and $q^{(2)} = -11.6$, the transverse shear strain energy is 43 percent of the total strain energy. (The shear correction factor in the constitutive relations is taken to be 5/6.) The respective extensional and bending energies at the same values of $q^{(1)}$ and $q^{(2)}$ are 21 percent and 6 percent of the total strain energy.

The accuracy of the maximum radial displacement u_c and of the total strain energy U obtained by using six MD2-1 elements, three MD3-2 elements, and two MD4-3 elements in half the meridian ($\xi = 0$ to $\xi = 1.0$) is indicated in figure 11. In this case, for the same total number of degrees of freedom, the accuracy of the mixed models is insensitive to the degree of interpolation functions used.

Accuracy of Degrees-of-Freedom Reduction Technique

In order to assess the accuracy and effectiveness of the reduction method when applied in conjunction with the mixed models, the isotropic circular toroid considered in a preceding subsection is analyzed with this method. Typical results are presented in figure 12. The structure is modeled by using 24 MD3-2 elements in half the meridian (with a total of 143 nonzero displacement degrees of freedom and 288 stress-resultant degrees of freedom). Nine basis vectors (path derivatives with respect to a generalized arc length in the solution space; see ref. 9) are generated for the unloaded structure ($q = 0$, $\{\bar{H}\} = 0$, and $\{\bar{X}\} = 0$) and are thus obtained by solving a linear set of finite-element equations. (See appendix B.) The basis vectors are orthonormalized with the Gram-Schmidt procedure in order to improve the conditioning of the reduced equations. As a measure of the error of the reduced equations, a weighted Euclidean norm of the residual vectors $\{R\}$ and $\{\bar{R}\}$ is introduced, namely

$$e = \frac{1}{q\ (6\bar{\delta} + 3\bar{m})} \sqrt{\{\bar{R}\}^t\ \{\bar{R}\} + \{R\}^t\ \{R\}} \tag{31}$$

where

$$\{\bar{R}\} = -[\bar{F}]\ \{\bar{H}\} + [\bar{S}]\ \{\bar{X}\} + \{\bar{G}(\bar{X})\} - \{\bar{R}\} \tag{32}$$

$$\{R\} = [\bar{S}^t]\ \{\bar{H}\} + \{\bar{m}\ (\bar{H},\bar{X})\} - q\ \{\bar{Q}(\bar{X})\} \tag{33}$$

The terms $6\bar{\delta}$ and $3\bar{m}$ are the total number of stress-resultant parameters and displacement degrees of freedom in the model. The error norm e is monitored and the basis vectors are updated when e exceeds the prescribed tolerance of 0.005. Nine new basis vectors are generated at $w_c/h = -3.29$. The new basis vectors are used to advance the solution up to $w_c/h = -12.0$. The error norm is less than the prescribed tolerance up to that value of w_c.

As can be seen in figure 12, the agreement between the solutions with the full system and the reduction technique is remarkably good except in the region just before the point of updating the vectors. (Updating of basis vectors is indicated by dotted lines between points.) Accurate solutions in that region can be obtained by using the updated (new) basis vectors through backtracking the solution path. At $w_c/h = -12.0$ and $Ua/Eh^4 = 320.0$, the errors in the displacement w_c and in the total strain energy U are 0.1 percent and 0.3 percent.

Accuracy of Model Size Reduction Technique

As a demonstration of the effectiveness of the procedure outlined in a previous section for reducing the size of the analysis model, consider the laminated anisotropic elliptical toroid shell shown in figure 8. The shell has clamped edges and is subjected to combined hydrostatic pressure (live load) and asymmetric ring load. (See fig. 13.) The hydrostatic pressure is uniform and has an intensity p_o/E_L of 0.66×10^{-3} per unit area of the deforming middle surface of the shell and remains

normal to that surface. The ring load is *normal to the undeformed middle surface* of the shell and is assumed to *retain its original direction throughout the analysis.* The response of the elliptical toroid shell along with the deformed configurations at three different values of the ring load are shown in figure 13. The shear correction factors in the constitutive relations are taken to be 5/6, and the transverse shear strain energy becomes the dominant energy (over 50 percent of the total strain energy) at $w_c/h = -0.9$ and reaches 90 percent of the total strain energy at $w_c/h = -5.0$.

The asymmetric ring load is decomposed into symmetric and antisymmetric components as shown in figure 2. The two path parameters λ_1 and λ_2 are selected to be the two load parameters $q^{(1)}$ and $q^{(2)}$ associated with the symmetric and antisymmetric ring load components. Ten basis vectors are generated at zero values of λ_1 and λ_2 (but at uniform nonzero p_o, resulting in a symmetric configuration). The basis vectors include the nonlinear solution ($\{\bar{H}\}$ and $\{\bar{X}\}$) evaluated at $q = P a/E_L h^3 = 0$, $q^{(1)} = q^{(2)} = 0$, and $p_o/E_L = 0.66 \times 10^{-3}$ and all its first, second, and third derivatives with respect to λ_1 and λ_2. These basis vectors and the reduced equations were generated by *using only half the shell meridian,* and the symmetry conditions (eqs. (30)) were applied at the centerline.

The accuracy of the solutions obtained with the foregoing procedure for the range $0 \leq |q| \leq 28.0$ is indicated in figure 14. Note that the same set of basis vectors is used throughout the analysis, and the error norm is found to be less than the prescribed tolerance of 0.005. At $q = -26.3$, the maximum errors in the displacement w_c and the total strain energy U are 0.9 percent and 2.0 percent.

For comparison, the single-parameter reduction method is applied to this problem. Four, five, and six basis vectors (path derivatives with respect to q) are generated at $q = 0$ ($p_o/E_L = 0.66 \times 10^{-3}$). *The generation of these basis vectors and the associated reduced equations require the use of the entire shell meridian.* The accuracy of the predictions of the single-parameter reduction method with four, five, and six vectors is given in figure 14. As can be seen in figure 14, the solutions obtained with four vectors are inaccurate for $|q| \geq 13.0$. On the other hand, the solutions with five and six vectors are highly accurate throughout the load range considered. Since the major cost of the analysis is that of generating the basis vectors and the reduced equations, the two-parameter reduction method is computationally more efficient than that of the single-parameter method.

DISCUSSION OF COMPUTATIONAL STRATEGY

The numerical results presented in this paper clearly demonstrate the accuracy and effectiveness of the proposed computational strategy for predicting the nonlinear, large-rotation, axisymmetric response of tires. In particular, the following comments regarding the mixed models and reduction technique are in order:

1. In spite of the equivalence discussed in the section entitled "Equivalence Between Mixed Models and Displacement Models," the mixed models developed herein combine the following advantages over their equivalent displacement models:

   A. The development of mixed models is simpler and more straightforward than that of the displacement models. This is particularly true for large-rotation and large-strain problems for which the functional of the mixed variational principle is simpler than that of the minimum potential energy principle.

B. The evaluation of the element characteristic arrays for the mixed models and their combinations to form the arrays $\mathbb{K}_{ij}$, $\mathbb{A}_i^{(\alpha)}$, $\mathbb{B}_{ij}^{(\alpha)}$, $\mathbb{C}_{ijk}^{(\alpha)}$, $\mathbb{D}_i^{(\alpha,\beta)}$, $\mathbb{E}_{ij}^{(\alpha,\beta)}$, and $\mathbb{F}_{ijk}^{(\alpha,\beta)}$ (and their counterparts with bars and tildes) (see eqs. (11) to (20)) involves fewer arithmetic operations than the formulation of the corresponding arrays in the displacement models. Moreover, the effort required in evaluating the aforementioned arrays can be reduced by selecting the interpolation functions for the stress resultants to be *orthonormal with respect to the weighting function* r, thereby simplifying the generation of $(F^{-1})_{IJ}$. (See appendix B.)

C. The elimination of the stress-resultant parameters H_I on the element level (condensation process) is similar to that used in hybrid models in which the stress-resultant field is described within the element and an independent displacement field is defined on the element boundaries. However, the present mixed models differ from hybrid models in the fact that both *stress-resultant and displacement fields are described within the element.*

D. If the stress resultants are eliminated on the element level, the present elements can be *viewed by a user as displacement models* and can be easily combined with other types of displacement elements to model a shell.

2. When reduction methods are used in conjunction with mixed models, the following two major advantages can be identified:

A. The arrays appearing in the finite-element equations of the mixed models have a *simpler form* than the corresponding arrays of the displacement models, and the evaluation of the path derivatives involves fewer arithmetic operations than that of the corresponding displacement models.

B. *The accuracy of the reduction method when used in conjunction with the mixed models is expected to be higher* than that of the corresponding displacement method (based on using the same number of basis vectors). This is particularly true for the stress resultants and is attributed to the fact that the path derivatives of both the stress resultants and the displacements are used as basis vectors. As a consequence of this, the basis vectors in the mixed method are less frequently updated than those in the displacement method.

3. The procedure outlined for reducing the size of the finite-element model of a symmetric shell through the decomposition of the asymmetric load into symmetric and antisymmetric components coupled with the use of the multiple-parameter reduction technique can lead to more dramatic savings in computational effort for nonaxisymmetric-response studies. Moreover, the same procedure can be applied when the initial discretization is done with numerical and approximation techniques rather than with finite elements.

CONCLUDING REMARKS

An effective computational strategy has been presented for the large-rotation nonlinear analysis of shells of revolution with application to tires. A total Lagrangian description of the shell deformation is used, and the analytical

formulation is based on a form of Reissner's large-deformation theory, including the effects of transverse shear deformation, laminated orthotropic material response, and moments acting about the normal to the middle surface. Only axisymmetric deformations of the shell are considered, and the load can be displacement dependent as well as nonconservative. The generalized stiffness coefficients (element characteristic arrays) are obtained by using the Hellinger-Reissner mixed variational principle. The polynomial interpolation (or shape) functions used for approximating the stress resultants are of lower degree than those used for approximating the generalized displacements. The three key components of the presented computational strategy are as follows: (1) use of mixed finite-element models with discontinuous stress resultants at the element interfaces, thereby allowing the elimination of these stress resultants on the element level; (2) considerable reduction in the total number of degrees of freedom through the use of a multiple-parameter reduction technique based on perturbation expansion; and (3) reduction in the size of the analysis model through the decomposition of asymmetric loads into symmetric and antisymmetric components coupled with the use of the multiple-parameter reduction technique.

Numerical results have been presented for toroidal and spherical shells subjected to constant-directional and follower forces (live loads). These examples demonstrate the high accuracy of the mixed models and show the effectiveness of using the presented computational strategy with these models.

Langley Research Center
National Aeronautics and Space Administration
Hampton, VA 23665
August 1, 1984

APPENDIX A

FUNDAMENTAL EQUATIONS OF THE NONLINEAR THEORY OF SHELLS OF REVOLUTION

The fundamental equations of Reissner's large-deformation theory for shells of revolution are given in reference 2 and are summarized herein. Only axisymmetric deformations are considered, and the effects of laminated orthotropic material response, transverse shear deformation, and moments turning around the normal to the middle surface are included. A total Lagrangian description of the shell deformation is used, and the shell configurations at different load levels are referred to the initial coordinate system of the undeformed shell.

Strain-Displacement Relationships

The relationships between the strains and the generalized displacements of the middle surface of the shell are given by

$$\varepsilon_s = \cos(\phi + \phi_o)\ \partial u - \sin(\phi + \phi_o)\ \partial w + \cos\phi - 1 = (1 + \varepsilon_{so})\cos\gamma_o - 1 \tag{A1}$$

$$\varepsilon_\theta = \frac{u}{r} \tag{A2}$$

$$\kappa_s = \partial\phi \tag{A3}$$

$$\kappa_\theta = \frac{1}{r}\left[\sin(\phi + \phi_o) - \sin\phi_o\right] \tag{A4}$$

$$\gamma = \sin(\phi + \phi_o)\ \partial u + \cos(\phi + \phi_o)\ \partial w + \sin\phi = (1 + \varepsilon_{so})\sin\gamma_o \tag{A5}$$

$$\lambda = \frac{1}{r}\left[\cos(\phi + \phi_o) - \cos\phi_o\right] \tag{A6}$$

where ε_{so} and ε_θ are the extensional strains in the meridional and circumferential directions; κ_s and κ_θ are the bending strains in the meridional and circumferential directions; γ_o is the transverse shearing strain; λ is the bending strain associated with the moment turning about the normal to the middle surface of the shell; ε_s and γ are virtual extensional and shearing strains; and $\partial \equiv d/ds$.

Constitutive Relations

The shell is assumed to be made of an orthotropic, linearly elastic material, and the relationships between the stress resultants and the strain measures of the shell are given by

$$\begin{bmatrix} \varepsilon_s \\ \varepsilon_\theta \\ \hline \kappa_s \\ \kappa_\theta \\ \hline \gamma \\ \lambda \end{bmatrix} = \left[\begin{array}{cc|cc|cc} a_{11} & a_{12} & b_{11} & b_{12} & 0 & 0 \\ & a_{22} & b_{12} & b_{22} & 0 & 0 \\ \hline & & g_{11} & g_{12} & 0 & 0 \\ & & & g_{22} & 0 & 0 \\ \hline & & & & a_s & 0 \\ \multicolumn{2}{c|}{\text{Symm.}} & & & & g_n \end{array}\right] \begin{bmatrix} N_s \\ N_\theta \\ \hline M_s \\ M_\theta \\ \hline Q \\ M_n \end{bmatrix} \qquad \text{(A7)}$$

where $a_{\alpha\beta}$, $b_{\alpha\beta}$, $g_{\alpha\beta}$ (for $\alpha,\beta = 1$ or 2), a_s, and g_n are shell compliance coefficients (inverses of shell stiffnesses). In the present study, the stiffness coefficient associated with M_n is set equal to the stiffness coefficient associated with M_θ. Both stiffness coefficients are obtained by inverting the matrix on the right-hand side of equation (A7).

APPENDIX B

FORMULAS FOR COEFFICIENTS IN THE FINITE-ELEMENT EQUATIONS FOR INDIVIDUAL ELEMENTS

The explicit forms of the arrays F_{IJ}, S_{Ij}, R_I, $A_I^{(\alpha)}$, $\bar{A}_I^{(\alpha)}$, $B_{Ij}^{(\alpha)}$, $\bar{B}_{Ij}^{(\alpha)}$, $T_i^{(\alpha)}$, P_i, and Q_{ij} are given in this appendix. For convenience, each of these arrays is partitioned into blocks corresponding to contributions from individual nodes or stress-resultant approximation functions. The expressions of the typical partitions (or blocks) are given in tables B1 and B2. Note that the order of the stress-resultant parameters in these partitions is N_s, N_θ, M_s, M_θ, Q_s, and M_n. The order of the nodal displacement parameters is u, w, and ϕ.

In tables B1 and B2, $\bar{N}_{i'}$ and $N_{j'}$ are respective interpolation functions for the stress resultants and the generalized displacements; r is the radial coordinate; m is the number of displacement nodes in the element; δ is the number of parameters used in approximating each of the stress resultants; $s^{(e)}$ is the element domain; $W^{(\alpha)}$ is the quadrature weighting coefficient (including a factor of 2π and the length of the element) at the numerical quadrature point α; and $\partial \equiv d/ds$. The range of the indices i' and j' is 1 to δ, and the range of the indices i' and j' is 1 to m. Note that $\sum_\alpha A_I^{(\alpha)} = R_I$.

APPENDIX B

TABLE B1.- EXPLICIT FORM OF TYPICAL PARTITIONS OF THE F, S, R, A, $\bar{A}$, B, $\bar{B}$, AND T ARRAYS

Array	Number of partitions (or blocks)	Typical partition
F_{IJ}	$\delta \times \delta$	$2\pi \int_{s(e)} \bar{N}_{i'} \bar{N}_{j'} r \begin{bmatrix} a_{11} & a_{12} & b_{11} & b_{12} & 0 & 0 \\ & a_{22} & b_{12} & b_{22} & 0 & 0 \\ & & g_{11} & g_{12} & 0 & 0 \\ & & & g_{22} & 0 & 0 \\ & & & & a_s & 0 \\ \text{Symm.} & & & & & g_n \end{bmatrix} ds$
S_{Ij}	$\delta \times m$	$2\pi \int_{s(e)} \bar{N}_{i'} \begin{bmatrix} 0 & 0 & 0 \\ N_{j'} & 0 & 0 \\ 0 & 0 & r \frac{\partial N_{j'}}{} \\ 0 & 0 & 0 \\ 0 & 0 & 0 \\ 0 & 0 & 0 \end{bmatrix} ds$
R_I	δ	$2\pi \int_{s(e)} \bar{N}_{i'} \begin{bmatrix} r \\ 0 \\ 0 \\ \sin \phi_o \\ 0 \\ \cos \phi_o \end{bmatrix} ds$

TABLE B1.- Continued

Array	Number of partitions (or blocks)	Typical partition
$A_I^{(\alpha)}$	δ	$w^{(\alpha)}\ \bar{N}_{i'}^{(\alpha)} \begin{bmatrix} r^{(\alpha)} \\ 0 \\ 0 \\ \sin\phi_o^{(\alpha)} \\ 0 \\ \cos\phi_o^{(\alpha)} \end{bmatrix}$
$\bar{A}^{(\alpha)}$	δ	$w^{(\alpha)}\ \bar{N}_{i'}^{(\alpha)} \begin{bmatrix} 0 \\ 0 \\ 0 \\ \cos\phi_o^{(\alpha)} \\ r^{(\alpha)} \\ \sin\phi_o^{(\alpha)} \end{bmatrix}$
$B_{Ij}^{(\alpha)}$	$\delta \times m$	$w^{(\alpha)}\ \bar{N}_{i'}^{(\alpha)}\ \partial N_{j'}^{(\alpha)}\ r^{(\alpha)} \begin{bmatrix} \cos\phi_o^{(\alpha)} & -\sin\phi_o^{(\alpha)} & 0 \\ 0 & 0 & 0 \\ 0 & 0 & 0 \\ 0 & 0 & 0 \\ \sin\phi_o^{(\alpha)} & \cos\phi_o^{(\alpha)} & 0 \\ 0 & 0 & 0 \end{bmatrix}$

TABLE B1.- Concluded

Array	Number of partitions (or blocks)	Typical partition
$\bar{B}_{Ij}^{(\alpha)}$	$s \times m$	$W^{(\alpha)}\ \bar{N}_{i,}^{(\alpha)}\ \partial N_{j,}^{(\alpha)}\ r^{(\alpha)}$ $\begin{bmatrix} -\sin\phi_o^{(\alpha)} & -\cos\phi_o^{(\alpha)} & 0 \\ 0 & 0 & 0 \\ 0 & 0 & 0 \\ 0 & 0 & 0 \\ \cos\phi_o^{(\alpha)} & -\sin\phi_o^{(\alpha)} & 0 \\ 0 & 0 & 0 \end{bmatrix}$
$T_i^{(\alpha)}$	m	$\begin{Bmatrix} 0 \\ 0 \\ N_{i,}^{(\alpha)} \end{Bmatrix}$

TABLE B2.- EXPLICIT FORM OF TYPICAL PARTITIONS OF THE P_i AND Q_{ij} ARRAYS FOR UNIFORM HYDROSTATIC PRESSURE (LIVE LOAD, $q = p_o$)

Array	Number of partitions (or blocks)	Typical partition
Q_{ij}	$m \times m$	$2\pi \int_{s(e)} \begin{bmatrix} N_{i,} N_{j,} \sin\phi_o & \partial N_{i,} N_{j,} r + N_{i,} N_{j,} \cos\phi_o & 0 \\ N_{i,} \partial N_{j,} r + N_{i,} N_{j,} \cos\phi_o & 0 & 0 \\ 0 & 0 & 0 \end{bmatrix} ds$
P_i	m	$2\pi \int_{s(e)} N_{i,} r \begin{Bmatrix} \sin\phi_o \\ \cos\phi_o \\ 0 \end{Bmatrix} ds$

APPENDIX C

EVALUATION OF PATH DERIVATIVES

The basis vectors are obtained by successively differentiating the governing finite-element equations (eqs. (24), obtained from eqs. (7) and (8)) with respect to the path parameters λ_1 and λ_2, assembling the resulting equations, and solving for the mixed partial path derivatives. For individual finite elements, the governing equations for the path derivatives $\frac{\partial^{m+n}}{\partial\lambda_1^m\,\partial\lambda_2^n} H_J$ and $\frac{\partial^{m+n}}{\partial\lambda_1^m\,\partial\lambda_2^n} X_j$ are

$$-F_{IJ}\frac{\partial^{m+n}}{\partial\lambda_1^m\,\partial\lambda_2^n} H_J + L_{Ij}\frac{\partial^{m+n}}{\partial\lambda_1^m\,\partial\lambda_2^n} X_j = \bar{V}_I^{(m,n)} \tag{C1}$$

$$L_{Ji}\frac{\partial^{m+n}}{\partial\lambda_1^m\,\partial\lambda_2^n} H_J + \left(M_{ij} - q^{(1)}\,Q_{ij}^{(1)} - q^{(2)}\,Q_{ij}^{(2)}\right)\frac{\partial^{m+n}}{\partial\lambda_1^m\,\partial\lambda_2^n} X_j = V_i^{(m,n)} \tag{C2}$$

where

$$L_{Ij} = S_{Ij} + \sum_\alpha \left\{\left[B_{Ij}^{(\alpha)} + T_j^{(\alpha)}\left(\bar{A}_I^{(\alpha)} + \bar{B}_{I\ell}^{(\alpha)}\,X_\ell\right)\right]\cos\phi^{(\alpha)} + \left[\bar{B}_{Ij}^{(\alpha)} - T_j^{(\alpha)}\left(A_I^{(\alpha)} + B_{I\ell}^{(\alpha)}\,X_\ell\right)\right]\sin\phi^{(\alpha)}\right\} \tag{C3}$$

$$M_{ij} = \sum_\alpha \left\{\left[T_i^{(\alpha)}\,\bar{B}_{Ij}^{(\alpha)} + T_j^{(\alpha)}\,\bar{B}_{Ii}^{(\alpha)} - T_i^{(\alpha)}\,T_j^{(\alpha)}\left(A_I^{(\alpha)} + B_{I\ell}^{(\alpha)}\,X_\ell\right)\right] H_I\cos\phi^{(\alpha)} + \left[-T_i^{(\alpha)}\,B_{Ij}^{(\alpha)} - T_j^{(\alpha)}\,B_{Ii}^{(\alpha)} - T_i^{(\alpha)}\,T_j^{(\alpha)}\left(\bar{A}_I^{(\alpha)} + \bar{B}_{I\ell}^{(\alpha)}\,X_\ell\right)\right] H_I\sin\phi^{(\alpha)}\right\} \tag{C4}$$

and $\bar{V}_I^{(m,n)}$ and $V_i^{(m,n)}$ are functions of previously evaluated (i.e., lower order) path derivatives. Explicit forms for some low-order right-hand sides are as follows:

$$\bar{V}_I^{(1,0)} = \bar{V}_I^{(0,1)} = 0 \tag{C5}$$

$$\bar{V}_I^{(2,0)} = \sum_\alpha \left[A_I^{(\alpha)}\,\dot{\phi}^{(\alpha)}\,\dot{\phi}^{(\alpha)} - \bar{B}_{I\ell}^{(\alpha)}\left(2\,\dot{X}_\ell\,\dot{\phi}^{(\alpha)}\right)\right] \tag{C6}$$

$$\bar{V}_I^{(1,1)} = \sum_\alpha \left[A_I^{(\alpha)} \dot{\phi}^{(\alpha)} \acute{\phi}^{(\alpha)} - \bar{B}_{I\ell}^{(\alpha)} \left(\dot{X}_\ell \acute{\phi}^{(\alpha)} + \acute{X}_\ell \dot{\phi}^{(\alpha)} \right) \right] \tag{C7}$$

$$\bar{V}_I^{(3,0)} = \sum_\alpha \left[A_I^{(\alpha)} \left(3 \ddot{\phi}^{(\alpha)} \dot{\phi}^{(\alpha)} \right) + \bar{A}_I^{(\alpha)} \dot{\phi}^{(\alpha)} \dot{\phi}^{(\alpha)} \dot{\phi}^{(\alpha)} + B_{I\ell}^{(\alpha)} \left(3 \dot{X}_\ell \dot{\phi}^{(\alpha)} \dot{\phi}^{(\alpha)} \right) - \bar{B}_{I\ell}^{(\alpha)} \left(3 \ddot{X}_\ell \dot{\phi}^{(\alpha)} + 3 \dot{X}_\ell \ddot{\phi}^{(\alpha)} \right) \right] \tag{C8}$$

$$\bar{V}_I^{(2,1)} = \sum_\alpha \left[A_I^{(\alpha)} \left(2 \dot{\acute{\phi}}^{(\alpha)} \dot{\phi}^{(\alpha)} + \ddot{\phi}^{(\alpha)} \acute{\phi}^{(\alpha)} \right) + \bar{A}_I^{(\alpha)} \dot{\phi}^{(\alpha)} \dot{\phi}^{(\alpha)} \acute{\phi}^{(\alpha)} + B_{I\ell}^{(\alpha)} \left(2 \dot{X}_\ell \dot{\phi}^{(\alpha)} \acute{\phi}^{(\alpha)} + \acute{X}_\ell \dot{\phi}^{(\alpha)} \dot{\phi}^{(\alpha)} \right) - \bar{B}_{I\ell}^{(\alpha)} \left(2 \dot{\acute{X}}_\ell \dot{\phi}^{(\alpha)} + \ddot{X}_\ell \acute{\phi}^{(\alpha)} + 2 \dot{X}_\ell \dot{\acute{\phi}}^{(\alpha)} + \acute{X}_\ell \ddot{\phi}^{(\alpha)} \right) \right] \tag{C9}$$

$$V_i^{(1,0)} = \dot{q}^{(1)} \left(P_i^{(1)} + Q_{ij}^{(1)} X_j \right) \tag{C10}$$

$$V_i^{(2,0)} = \ddot{q}^{(1)} \left(P_i^{(1)} + Q_{ij}^{(1)} X_j \right) + 2 \dot{q}^{(1)} Q_{ij}^{(1)} \dot{X}_j + \sum_\alpha \left[C_{iJ}^{(\alpha)} H_J \dot{\phi}^{(\alpha)} \dot{\phi}^{(\alpha)} - \bar{C}_{Ij}^{(\alpha)} \left(2 \dot{H}_J \dot{\phi}^{(\alpha)} \right) + T_i^{(\alpha)} B_{J\ell}^{(\alpha)} \left(2 H_J \dot{X}_\ell \dot{\phi}^{(\alpha)} + 2 \dot{H}_J X_\ell \dot{\phi}^{(\alpha)} \right) - T_i^{(\alpha)} \bar{B}_{J\ell}^{(\alpha)} \left(2 \dot{H}_J \dot{X}_\ell - H_J X_\ell \dot{\phi}^{(\alpha)} \dot{\phi}^{(\alpha)} \right) \right] \tag{C11}$$

$$V_i^{(1,1)} = \dot{q}^{(1)} Q_{ij}^{(1)} \acute{X}_j + \acute{q}^{(2)} Q_{ij}^{(2)} \dot{X}_j + \sum_\alpha \left[C_{iJ}^{(\alpha)} H_J \dot{\phi}^{(\alpha)} \acute{\phi}^{(\alpha)} - \bar{C}_{iJ}^{(\alpha)} \left(\dot{H}_J \acute{\phi}^{(\alpha)} + \acute{H}_J \dot{\phi}^{(\alpha)} \right) + T_i^{(\alpha)} B_{J\ell}^{(\alpha)} \left(H_J \dot{X}_\ell \acute{\phi}^{(\alpha)} + H_J \acute{X}_\ell \dot{\phi}^{(\alpha)} + \dot{H}_J X_\ell \acute{\phi}^{(\alpha)} + \acute{H}_J X_\ell \dot{\phi}^{(\alpha)} \right) - T_i^{(\alpha)} \bar{B}_{J\ell}^{(\alpha)} \left(\dot{H}_J \acute{X}_\ell + \acute{H}_J \dot{X}_\ell - H_J X_\ell \dot{\phi}^{(\alpha)} \acute{\phi}^{(\alpha)} \right) \right] \tag{C12}$$

$$
\begin{aligned}
V_i^{(3,0)} = {} & \dddot{q}^{(1)} \left(P_i^{(1)} + Q_{ij}^{(1)} X_j \right) + 3 \ddot{q}^{(1)} Q_{ij}^{(1)} \dot{X}_j + 3 \dot{q}^{(1)} Q_{ij}^{(1)} \ddot{X}_j \\
& + \sum_{\alpha} \Big[C_{iJ}^{(\alpha)} \left(3 \dot{H}_J \dot{\phi}^{(\alpha)} \dot{\phi}^{(\alpha)} + 3 H_J \ddot{\phi}^{(\alpha)} \dot{\phi}^{(\alpha)} \right) \\
& - \bar{C}_{iJ}^{(\alpha)} \left(3 \ddot{H}_J \dot{\phi}^{(\alpha)} + 3 \dot{H}_J \ddot{\phi}^{(\alpha)} - H_J \dot{\phi}^{(\alpha)} \dot{\phi}^{(\alpha)} \dot{\phi}^{(\alpha)} \right) \\
& + T_i^{(\alpha)} B_{J\ell}^{(\alpha)} \left(3 H_J \ddot{X}_\ell^{(\alpha)} \dot{\phi}^{(\alpha)} + 6 \dot{H}_J \dot{X}_\ell \dot{\phi}^{(\alpha)} + 3 H_J \dot{X}_\ell \ddot{\phi}^{(\alpha)} \right. \\
& \left. + 3 \ddot{H}_J X_\ell \dot{\phi}^{(\alpha)} + 3 \dot{H}_J X_\ell \ddot{\phi}^{(\alpha)} - H_J X_\ell \dot{\phi}^{(\alpha)} \dot{\phi}^{(\alpha)} \dot{\phi}^{(\alpha)} \right) \\
& - T_i^{(\alpha)} \bar{B}_{J\ell}^{(\alpha)} \left(3 \dot{H}_J \ddot{X}_\ell + 3 \ddot{H}_J \dot{X}_\ell - 3 H_J \dot{X}_\ell \dot{\phi}^{(\alpha)} \dot{\phi}^{(\alpha)} \right. \\
& \left. - 3 \dot{H}_J X_\ell \dot{\phi}^{(\alpha)} \dot{\phi}^{(\alpha)} - 3 H_J X_\ell \ddot{\phi}^{(\alpha)} \dot{\phi}^{(\alpha)} \right) \Big]
\end{aligned}
\tag{C13}
$$

$$
\begin{aligned}
V_i^{(2,1)} = {} & \ddot{q}^{(1)} Q_{ij}^{(1)} \acute{X}_j + 2 \dot{q}^{(1)} Q_{ij}^{(1)} \dot{\acute{X}}_j + \acute{q}^{(2)} Q_{ij}^{(2)} \ddot{X}_j \\
& + \sum_{\alpha} \Big[C_{iJ}^{(\alpha)} \left(2 \dot{H}_J \dot{\phi}^{(\alpha)} \acute{\phi}^{(\alpha)} + \acute{H}_J \dot{\phi}^{(\alpha)} \dot{\phi}^{(\alpha)} + H_J \ddot{\phi}^{(\alpha)} \acute{\phi}^{(\alpha)} \right. \\
& \left. + 2 H_J \dot{\acute{\phi}}^{(\alpha)} \dot{\phi}^{(\alpha)} \right) - \bar{C}_{iJ}^{(\alpha)} \left(\ddot{H}_J \acute{\phi}^{(\alpha)} + 2 \dot{\acute{H}}_J \dot{\phi}^{(\alpha)} + 2 \dot{H}_J \dot{\acute{\phi}}^{(\alpha)} \right. \\
& \left. + \acute{H}_J \ddot{\phi}^{(\alpha)} - H_J \dot{\phi}^{(\alpha)} \dot{\phi}^{(\alpha)} \acute{\phi}^{(\alpha)} \right) \\
& + T_i^{(\alpha)} B_{J\ell}^{(\alpha)} \left(H_J \ddot{X}_\ell \acute{\phi}^{(\alpha)} + 2 H_J \dot{\acute{X}}_\ell \dot{\phi}^{(\alpha)} + 2 \dot{H}_J \dot{X}_\ell \acute{\phi}^{(\alpha)} \right. \\
& + 2 \dot{H}_J \acute{X}_\ell \dot{\phi}^{(\alpha)} + 2 \acute{H}_J \dot{X}_\ell \dot{\phi}^{(\alpha)} + 2 H_J \dot{X}_\ell \dot{\acute{\phi}}^{(\alpha)} + H_J \acute{X}_\ell \ddot{\phi}^{(\alpha)} \\
& + 2 \dot{\acute{H}}_J X_\ell \dot{\phi}^{(\alpha)} + \ddot{H}_J X_\ell \acute{\phi}^{(\alpha)} + 2 \dot{H}_J X_\ell \dot{\acute{\phi}}^{(\alpha)} \\
& \left. + \acute{H}_J X_\ell \ddot{\phi}^{(\alpha)} - H_J X_\ell \dot{\phi}^{(\alpha)} \dot{\phi}^{(\alpha)} \acute{\phi}^{(\alpha)} \right) \\
& - T_i^{(\alpha)} \bar{B}_{J\ell}^{(\alpha)} \left(2 \dot{H}_J \dot{\acute{X}}_\ell + \acute{H}_J \ddot{X}_\ell + 2 \dot{\acute{H}}_J \dot{X}_\ell + \ddot{H}_J \acute{X}_\ell - 2 H_J \dot{X}_\ell \dot{\phi}^{(\alpha)} \acute{\phi}^{(\alpha)} \right. \\
& - H_J \acute{X}_\ell \dot{\phi}^{(\alpha)} \dot{\phi}^{(\alpha)} - 2 \dot{H}_J X_\ell \dot{\phi}^{(\alpha)} \acute{\phi}^{(\alpha)} - \acute{H}_J X_\ell \dot{\phi}^{(\alpha)} \dot{\phi}^{(\alpha)} \\
& \left. - 2 H_J X_\ell \dot{\acute{\phi}}^{(\alpha)} \dot{\phi}^{(\alpha)} - H_J X_\ell \ddot{\phi}^{(\alpha)} \acute{\phi}^{(\alpha)} \right) \Big]
\end{aligned}
\tag{C14}
$$

where

$$A_I^{(\alpha)} = \left(A_I^{(\alpha)} + B_{I\ell}^{(\alpha)} X_\ell\right) \cos \phi^{(\alpha)} + \left(\bar{A}_I^{(\alpha)} + \bar{B}_{I\ell}^{(\alpha)} X_\ell\right) \sin \phi^{(\alpha)} \tag{C15}$$

$$\bar{A}_I^{(\alpha)} = \left(\bar{A}_I^{(\alpha)} + \bar{B}_{I\ell}^{(\alpha)} X_\ell\right) \cos \phi^{(\alpha)} - \left(A_I^{(\alpha)} + B_{J\ell}^{(\alpha)} X_\ell\right) \sin \phi^{(\alpha)} \tag{C16}$$

$$\mathcal{B}_{I\ell}^{(\alpha)} = B_{I\ell}^{(\alpha)} \cos \phi^{(\alpha)} + \bar{B}_{I\ell}^{(\alpha)} \sin \phi^{(\alpha)} \tag{C17}$$

$$\bar{\mathcal{B}}_{I\ell}^{(\alpha)} = \bar{B}_{I\ell}^{(\alpha)} \cos \phi^{(\alpha)} - B_{I\ell}^{(\alpha)} \sin \phi^{(\alpha)} \tag{C18}$$

$$C_{iJ}^{(\alpha)} = \left(B_{Ji}^{(\alpha)} + T_i^{(\alpha)} \bar{A}_J^{(\alpha)}\right) \cos \phi^{(\alpha)} + \left(\bar{B}_{Ji}^{(\alpha)} - T_i^{(\alpha)} A_J^{(\alpha)}\right) \sin \phi^{(\alpha)} \tag{C19}$$

$$\bar{C}_{iJ}^{(\alpha)} = \left(\bar{B}_{Ji}^{(\alpha)} - T_i^{(\alpha)} A_J^{(\alpha)}\right) \cos \phi^{(\alpha)} - \left(B_{Ji}^{(\alpha)} + T_i^{(\alpha)} \bar{A}_J^{(\alpha)}\right) \sin \phi^{(\alpha)} \tag{C20}$$

A prescription for obtaining expressions for $\bar{V}_I^{(m,n)}$ and $V_i^{(m,n)}$ is the following: (1) begin with $-\bar{f}_I$ and $-f_i$ in equations (7) and (8); (2) form their (m,n)th derivatives; (3) set $\dfrac{\partial^{m+n}}{\partial\lambda_1^m \partial\lambda_2^n} H_J$ and $\dfrac{\partial^{m+n}}{\partial\lambda_1^m \partial\lambda_2^n} X_j$ to zero in these expressions; and (4) express the results in terms of the variables $A_I^{(\alpha)}$, $\bar{A}_I^{(\alpha)}$, ..., $\bar{C}_{iJ}^{(\alpha)}$ given by equations (C15) to (C20).

In equations (C6) to (C20), a dot ($\cdot$) over a symbol refers to a derivative with respect to λ_1, and a prime ($'$) over a symbol refers to a derivative with respect to λ_2. Superscript α denotes the value of the quantity at the numerical quadrature point α. The summation sign extends over all the numerical quadrature points. The range of uppercase indices is 1 to 6δ (where δ is the number of parameters used in approximating each one of the stress resultants), and the range of the lowercase indices is 1 to $3m$ (where m is the number of displacement nodes). In equations (C6) to (C12), it is assumed that $\dot{q}^{(1)} = \dot{q}^{(2)} = 0$. Note that the coefficients on the left-hand sides of equations (C1) and (C2), which must be factored, are the same for each of the path derivatives. Hence, the matrix of these equations is factored only once regardless of the number of path derivatives generated. If a large number of basis vectors are used, orthonormalization may be needed in order to improve the conditioning of the reduced system of equations.

APPENDIX C

If the path derivatives are generated at $\lambda_1 = \lambda_2 = 0$ (and $q^{(1)} = q^{(2)} = 0$), then $H_I = 0$ and $X_i = 0$, $\sin \phi^{(\alpha)} = \phi^{(\alpha)} = 0$. Equations (C3) to (C20) are thus considerably simplified, and the computational effort in evaluating the path derivatives is reduced. For nonconservative loading, the array Q_{ij} is asymmetric. However, the evaluation of the initial path derivatives $\left(\text{at } q^{(1)} = q^{(2)} = 0\right)$ *involves the decomposition of a symmetric matrix only.*

APPENDIX D

FORM OF THE REDUCED EQUATIONS

The governing equations used in evaluating the undetermined coefficients ψ_i (the unknowns of the reduced equations) have the following form:

$$\tilde{K}_{ij}\,\psi_j + \sum_{\alpha}\left(\left\{\tilde{A}_i^{(\alpha)} + \left[2\,\tilde{B}_{ij}^{(\alpha)} + \tilde{T}_i^{(\alpha)}\left(\tilde{\tilde{A}}_j^{(\alpha)} + \tilde{\tilde{B}}_{jk}^{(\alpha)}\,\psi_k\right)\right]\psi_j\right\}\cos\left(T_m^{(\alpha)}\,\psi_m\right)\right.$$

$$\left. + \left\{\tilde{\tilde{A}}_i^{(\alpha)} + \left[2\,\tilde{\tilde{B}}_{ij}^{(\alpha)} - \tilde{T}_i^{(\alpha)}\left(\tilde{A}_j^{(\alpha)} + \tilde{B}_{jk}^{(\alpha)}\,\psi_k\right)\right]\psi_j\right\}\sin\left(T_m^{(\alpha)}\,\psi_m\right)\right)$$

$$- \tilde{R}_i - q^{(1)}\left(\tilde{P}_i^{(1)} + \tilde{Q}_{ij}^{(1)}\,\psi_j\right) - q^{(2)}\left(\tilde{P}_i^{(2)} + \tilde{Q}_{ij}^{(2)}\,\psi_j\right) = 0 \qquad \text{(D1)}$$

where

$$\tilde{K}_{ij} = \sum_{\text{Elements}}\left(-\bar{\Gamma}_{Ii}\,F_{IJ}\,\bar{\Gamma}_{Jj} + \bar{\Gamma}_{Ii}\,S_{Ij}\,\Gamma_{jj} + \bar{\Gamma}_{Ij}\,S_{Ij}\,\Gamma_{ji}\right) \qquad \text{(D2)}$$

$$\tilde{A}_i^{(\alpha)} = \sum_{\text{Elements}}\bar{\Gamma}_{Ii}\,A_I^{(\alpha)} \qquad \text{(D3)}$$

$$\tilde{\tilde{A}}_i^{(\alpha)} = \sum_{\text{Elements}}\bar{\Gamma}_{Ii}\,\bar{A}_I^{(\alpha)} \qquad \text{(D4)}$$

$$\tilde{B}_{ij}^{(\alpha)} = \frac{1}{2}\sum_{\text{Elements}}\left(\bar{\Gamma}_{Ii}\,B_{Ij}^{(\alpha)}\,\Gamma_{jj} + \bar{\Gamma}_{Ij}\,B_{Ij}^{(\alpha)}\,\Gamma_{ji}\right) \qquad \text{(D5)}$$

$$\tilde{\tilde{B}}_{ij}^{(\alpha)} = \frac{1}{2}\sum_{\text{Elements}}\left(\bar{\Gamma}_{Ij}\,\bar{B}_{Ij}^{(\alpha)}\,\Gamma_{jj} + \bar{\Gamma}_{Ii}\,\bar{B}_{Ij}^{(\alpha)}\,\Gamma_{jj}\right) \qquad \text{(D6)}$$

$$\tilde{T}_i^{(\alpha)} = \sum_{\text{Elements}}\Gamma_{ji}\,T_j^{(\alpha)} \qquad \text{(D7)}$$

$$\tilde{R}_i = \sum_{\text{Elements}} \bar{\Gamma}_{Ii} R_I \tag{D8}$$

$$\tilde{P}_i^{(1)} = \sum_{\text{Elements}} \Gamma_{ji} P_j^{(1)} \tag{D9}$$

$$\tilde{Q}_{ij}^{(1)} = \sum_{\text{Elements}} \Gamma_{ii} \Gamma_{jj} Q_{ij}^{(1)} \tag{D10}$$

$$\tilde{P}_i^{(2)} = \sum_{\text{Elements}} \Gamma_{ji} P_j^{(2)} \tag{D11}$$

$$\tilde{Q}_{ij}^{(2)} = \sum_{\text{Elements}} \Gamma_{ii} \Gamma_{jj} Q_{ij}^{(2)} \tag{D12}$$

In equations (D1) to (D12), the range of the indices i, j, k, and m is 1 to n (the number of unknowns); the range of the uppercase indices is 1 to $6s$ (where s is the number of parameters used in approximating each of the stress resultants); the range of the lowercase indices is 1 to 3m (where m is the number of displacement nodes in the element); and a repeated subscript in the same term denotes summation over its full range. Superscripts within parentheses are not summed.

REFERENCES

1. Tanner, John A., compiler: Tire Modeling. NASA CP-2264, 1983.

2. Reissner, Eric: On Finite Symmetrical Deflections of Thin Shells of Revolution. Trans. ASME, Ser. E: J. Appl. Mech., vol. 36, no. 2, June 1969, pp. 267-270; vol. 39, no. 4, Dec. 1972, pp. 1137-1138.

3. Argyris, J. H.; Straub, K.; and Symeonidis, Sp.: Static and Dynamic Stability of Nonlinear Elastic Systems Under Nonconservative Forces - Natural Approach. Comput. Methods Appl. Mech. & Eng., vol. 32, nos. 1-3, Sept. 1982, pp. 59-83.

4. Malkus, David S.; and Hughes, Thomas J. R.: Mixed Finite Element Methods - Reduced and Selective Integration Techniques: A Unification of Concepts. Comput. Methods Appl. Mech. & Eng., vol. 15, no. 1, July 1978, pp. 63-81.

5. Noor, Ahmed K.; and Peters, Jeanne M.: Mixed Models and Reduced/Selective Integration Displacement Models for Nonlinear Analysis of Curved Beams. Int. J. Numer. Methods Eng., vol. 17, no. 4, Apr. 1981, pp. 615-631.

6. Noor, Ahmed K.; and Andersen, C. M.: Mixed Models and Reduced/Selective Integration Displacement Models for Nonlinear Shell Analysis. Int. J. Numer. Methods Eng., vol. 18, no. 10, Oct. 1982, pp. 1429-1454.

7. Noor, Ahmed K.; and Peters, Jeanne M.: Reduced Basis Technique for Nonlinear Analysis of Structures. AIAA J., vol. 18, no. 4, Apr. 1980, pp. 455-462.

8. Noor, Ahmed K.: Recent Advances in Reduction Methods for Nonlinear Problems. Comput. & Struct., vol. 13, no. 1-3, June 1981, pp. 31-44.

9. Noor, Ahmed K.; and Peters, Jeanne M.: Tracing Post-Limit-Point Paths With Reduced Basis Technique. Comput. Methods Appl. Mech. & Eng., vol. 28, no. 2, Sept. 1981, pp. 217-240.

10. Noor, Ahmed K.; and Peters, Jeanne M.: Recent Advances in Reduction Methods for Instability Analysis of Structures. Comput. & Struct., vol. 16, no. 1-4, 1983, pp. 67-80.

11. Noor, Ahmed K.; and Peters, Jeanne M.: Multiple-Parameter Reduced Basis Technique for Bifurcation and Post-Buckling Analyses of Composite Plates. Int. J. Numer. Methods Eng., vol. 19, no. 12, Dec. 1983, pp. 1783-1803.

12. Noor, A. K.; Peters, J. M.; and Andersen, C. M.: Mixed Models and Reduction Techniques for Large Rotation Nonlinear Problems. Computer Methods for Nonlinear Solids and Structural Mechanics, AMD - Vol. 54, Satya N. Atluri and Nicholas Perrone, eds., American Soc. Mech. Eng., c.1983, pp. 155-180.

13. Kalnins, A.; and Lestingi, J. F.: On Nonlinear Analysis of Elastic Shells of Revolution. Trans. ASME, Ser. E: J. Appl. Mech., vol. 34, no. 1, Mar. 1967, pp. 59-64.

14. Yaghmai, S.; and Popov, E. P.: Incremental Analysis of Large Deflections of Shells of Revolution. Int. J. Solids & Struct., vol. 7, no. 10, Oct. 1971, pp. 1375-1393.

15. Chan, A. S. L.; and Trbojevic, V. M.: Thin Shell Finite Element by the Mixed Method Formulation - Parts 2 and 3. Comput. Methods Appl. Mech. & Eng., vol. 10, no. 1, Jan. 1977, pp. 75-103.

16. Mescall, J. F.: Large Deflections of Spherical Shells Under Concentrated Loads. Trans. ASME, Ser. E: J. Appl. Mech., vol. 32, no. 4, 1965, pp. 936-938.

17. Parisch, H.: Geometrical Nonlinear Analysis of Shells. Comput. Methods Appl. Mech. & Eng., vol. 14, no. 2, May 1978, pp. 159-178.

18. Sanders, J. Lyell, Jr.: Nonlinear Theories for Thin Shells. Quart. Appl. Math., vol. XXI, no. 1, Apr. 1963, pp. 21-36.

19. Budiansky, Bernard: Notes on Nonlinear Shell Theory. Trans. ASME, Ser. E: J. Appl. Mech., vol. 35, no. 2, June 1968, pp. 393-401.

SYMBOLS

$A_I^{(\alpha)}, \bar{A}_I^{(\alpha)}, B_{Ij}^{(\alpha)}, \bar{B}_{Ij}^{(\alpha)}$	multipliers of the trigonometric contributions to the finite-element equations for individual elements (see eqs. (7) and (8) and appendix B)
$A_I^{(\alpha)}, \bar{A}_I^{(\alpha)}, B_{I\ell}^{(\alpha)}, \bar{B}_{I\ell}^{(\alpha)}, C_{iJ}^{(\alpha)}, \bar{C}_{iJ}^{(\alpha)}$	arrays defined in equations (C15) to (C20)
$\tilde{A}_i^{(\alpha)}, \tilde{\tilde{A}}_i^{(\alpha)}, \tilde{B}_{ij}^{(\alpha)}, \tilde{\tilde{B}}_{ij}^{(\alpha)}, \tilde{T}_i^{(\alpha)}, \tilde{R}_i$	reduced-equation arrays defined in equations (D3) to (D8)
$\mathbf{A}_i^{(\alpha)}, \mathbf{B}_{ij}^{(\alpha)}, \mathbf{C}_{ijk}^{(\alpha)}, \bar{\mathbf{A}}_i^{(\alpha)}, \bar{\mathbf{B}}_{ij}^{(\alpha)}, \bar{\mathbf{C}}_{ijk}^{(\alpha)}, \mathbf{D}_i^{(\alpha,\beta)}, \mathbf{E}_{ij}^{(\alpha,\beta)}, \mathbf{F}_{ijk}^{(\alpha,\beta)}, \bar{\mathbf{D}}_i^{(\alpha,\beta)}, \bar{\mathbf{E}}_{ij}^{(\alpha,\beta)}, \bar{\mathbf{F}}_{ijk}^{(\alpha,\beta)}, \tilde{\mathbf{D}}_i^{(\alpha,\beta)}, \tilde{\mathbf{E}}_{ij}^{(\alpha,\beta)}, \tilde{\mathbf{F}}_{ijk}^{(\alpha,\beta)}$	elemental arrays (see eqs. (12) to (21)
a	radial distance for toroidal shell (see fig. 3)
$a_{11}, a_{12}, a_{22}, a_s, b_{11}, b_{12}, b_{22}, g_{11}, g_{12}, g_{22}, g_n$	shell compliance coefficients (inverses of shell stiffnesses)
E	Young's modulus of isotropic material
E_L, E_T	elastic moduli in direction of fibers and normal to it
e	error norm
F_{IJ}	linear flexibility coefficients
$[\bar{\mathcal{F}}], [\bar{\mathcal{S}}]$	global matrices defined in equations (24)
$\bar{f}_I, f_i$	arrays defined in equations (7) and (8)
G_{LT}, G_{TT}	shear moduli in plane of fibers and normal to it
$\{\bar{\mathfrak{C}}\}, \{\bar{\mathfrak{M}}\}$	global vectors of trigonometric contributions in ϕ
H_I	stress-resultant parameters
$\{\bar{H}\}$	assembled vector of stress-resultant parameters

h	total thickness of the shell
$\tilde{K}_{ij}$	linear stiffness arrays of the reduced equations (see eq. (D2))
K_{ij}	linear element coefficients defined in equation (11)
$\overset{*}{K}_{ij}$	linear stiffness coefficients for individual elements (see eq. (23))
L_{Ij}, M_{ij}	generalized stiffness coefficients defined in equations (C3) and (C4)
M_n	moment resultant turning about the normal to the middle surface of the shell
M_s, M_θ	meridional and circumferential (hoop) bending stress resultants
M	external meridional concentrated moment
m	number of displacement nodes in an element
$\bar{m}$	number of displacement nodes in the entire finite-element model
m	intensity of external meridional distributed moments
N_s, N_θ	meridional and circumferential (hoop) stress resultants
$N, \bar{N}$	shape (or interpolation) functions used in approximating the generalized displacements and stress resultants
n	number of quadrature points in an element
P	ring load
$P_i, P_i^{(1)}, P_i^{(2)}$	normalized load components
$\tilde{P}_i^{(1)}, \tilde{P}_i^{(2)}$	normalized load coefficients of the reduced equations
p_o	intensity of pressure load (internal pressures have positive sign)
p_u, p_w	intensity of distributed loads in the radial and axial directions of the shell
Q_s	transverse shear stress resultant
$Q_{ij}^{(1)}, Q_{ij}^{(2)}$	normalized load stiffness coefficients
$\tilde{Q}_{ij}^{(1)}$ $\tilde{Q}_{ij}^{(2)}$	load stiffness coefficients of the reduced equations
$\bar{Q}^{(1)}, \bar{Q}^{(2)}$	vectors of normalized external forces acting on the shell (see eqs. (24))
$q^{(1)}, q^{(2)}$	load parameters

R	radius of curvature of a spherical cap (see fig. 6)
R_I	integrals of shape functions (see eq. (7))
$\{\bar{R}\}$	constant vector assembled from the elemental contributions R_I (see eqs. (24))
r	radial coordinate of the shell
$\mathcal{r}$	number of basis vectors
S_{Ij}	linear strain-displacement coefficients of the shell element (see eqs. (7) and (8) and appendix B)
s	meridional coordinate of the shell
$\mathcal{s}$	number of parameters used in approximating each of the stress resultants within the individual elements
$\bar{\mathcal{s}}$	number of parameters used in approximating each of the stress resultants in the shell
$T_i^{(\alpha)}$	array defined in equation (9) and appendix B
U	total strain energy of the shell
u,w	radial and axial displacement components of the middle surface of the shell
$\bar{u},\bar{w}$	tangential and normal displacement components of the middle surface of the shell
$\bar{V}_I, V_i$	arrays defined in appendix C
w_c	axial displacement at point c
X_i	nodal displacements
$\{\bar{X}\}$	assembled vector of nodal displacements
x_1,x_2,x_3	Cartesian coordinate system, with x_3 coinciding with the axis of revolution of the shell
$\bar{\Gamma}_{I\mathcal{i}'}, \Gamma_{j\mathcal{i}'}$, $[\bar{\Gamma}], [\Gamma]$	matrices of basis vectors
γ_o	transverse shear strain
δ	variational operator
ε_s, γ	virtual extensional and shearing strains

ε_{so} extensional strain in the meridional direction

ε_{θ} extensional strain in the circumferential direction

θ circumferential (hoop) coordinate of the shell

κ_s, κ_θ meridional and circumferential (hoop) bending strains

λ bending strain associated with the moment turning about the normal to the shell M_n

λ_1, λ_2 path parameters

ν Poisson's ratio for isotropic material

ν_{LT} major Poisson's ratio of the individual layers of a laminated shell

ξ nondimensional meridional coordinate

$\Pi, \bar{\Pi}$ functionals defined in equations (1) and (2)

ϕ rotation of the shell middle surface

$\bar{\phi}$ $= \phi + \phi_o$

ϕ_o angle between the axis of revolution and the normal to the shell middle surface

ψ_i unknowns of the reduced equations

∂ $\equiv \frac{d}{ds}$

Ranges of indices:

I,J 1 to 6δ

$\bar{I},\bar{J}$ 1 to $6\bar{\delta}$

i,j,k,ℓ 1 to 3m

$\bar{i},\bar{j}$ 1 to $\bar{m}$

i′,j′ 1 to m

i,j,k,m 1 to r

i' j' 1 to δ

Finite-element model notation:

DEm — displacement model based on normal integration and having m displacement nodes

DRm-n — displacement model based on reduced integration; number of displacement nodes equals m; total number of quadrature points in reduced integration formula equals n

MDm-n — mixed model with discontinuous stress resultants at interelement boundaries and m displacement nodes; number of quadrature points in the Gauss-Legendre formula equals n; number of parameters δ used in approximating each of the stress resultants within the individual elements also equals n

MDm-m — mixed model with discontinuous stress resultants at interelement boundaries and m displacement nodes; number of quadrature points in the Gauss-Legendre formula equals m; number of parameters δ used in approximating each of the stress resultants within the individual elements also equals m

TABLE 1.- CHARACTERISTICS OF FINITE-ELEMENT MODELS USED IN THE PRESENT STUDY

(a) Mixed models

Stress-resultant approximation	Displacement approximation	Number of quadrature points	Designation (a)
Constant	Linear	1	MD2-1*
Linear	Quadratic	2	MD3-2**
Quadratic	Cubic	3	MD4-3†

(b) Displacement models

Displacement approximation	Number of quadrature points	Designation (a)
Linear	2	DE2
	1	DR2-1*
Quadratic	3	DE3
	2	DR3-2**
Cubic	4	DE4
	3	DR4-3†

[a]Symbols *, **, and † indicate equivalent finite-element models.

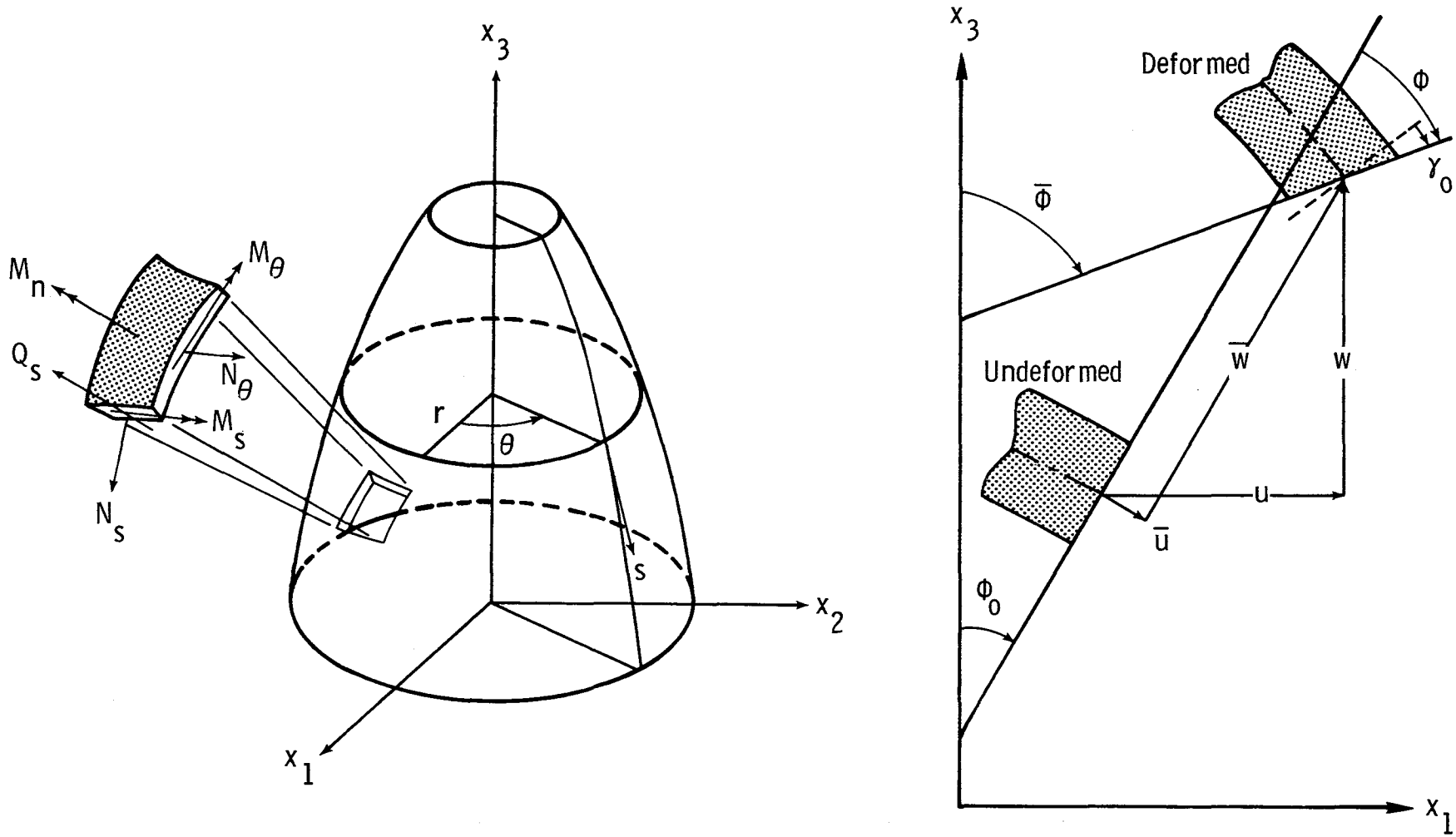

Figure 1.- Shell element and sign convention.

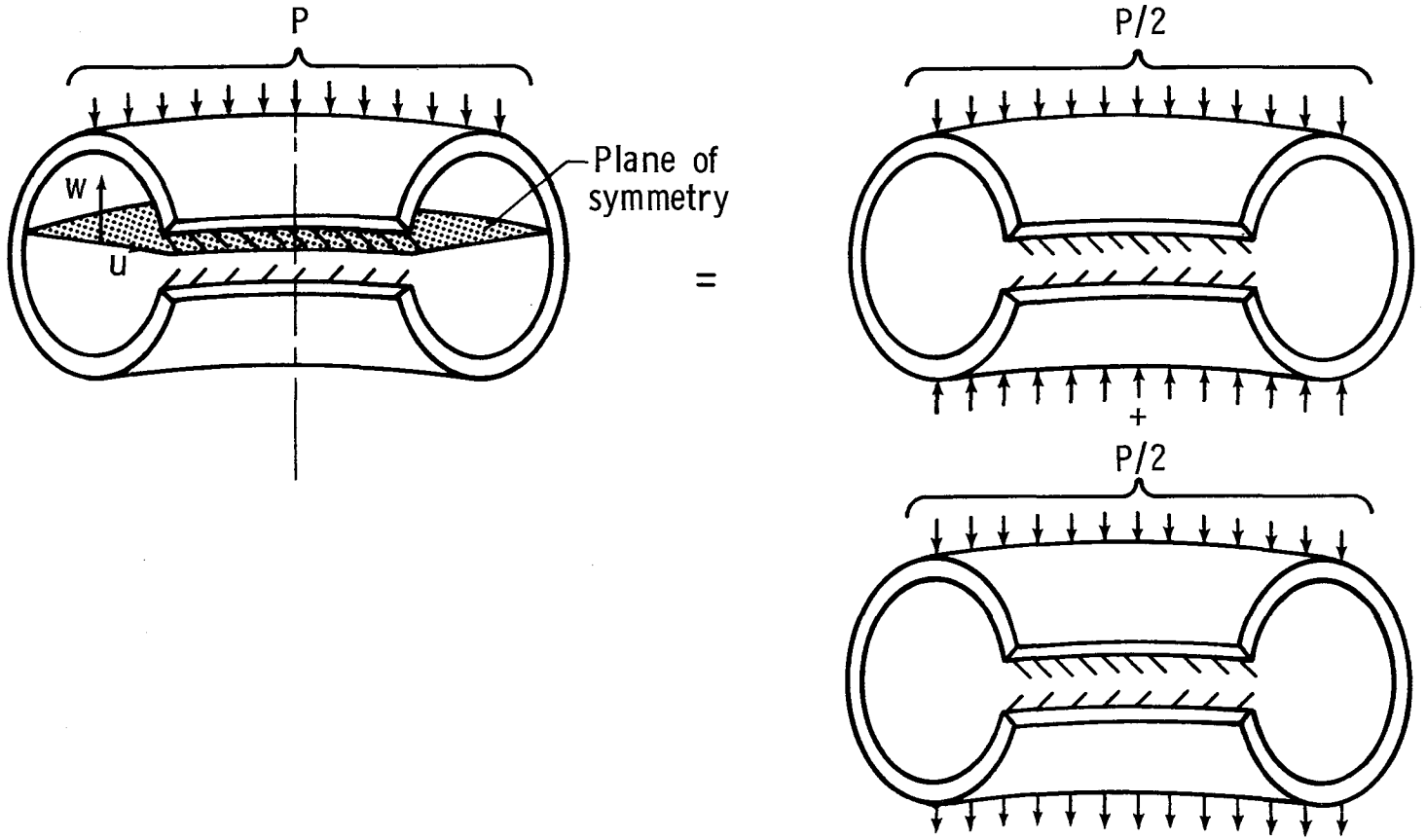

Figure 2.- Decomposition of ring load into symmetric and antisymmetric components.

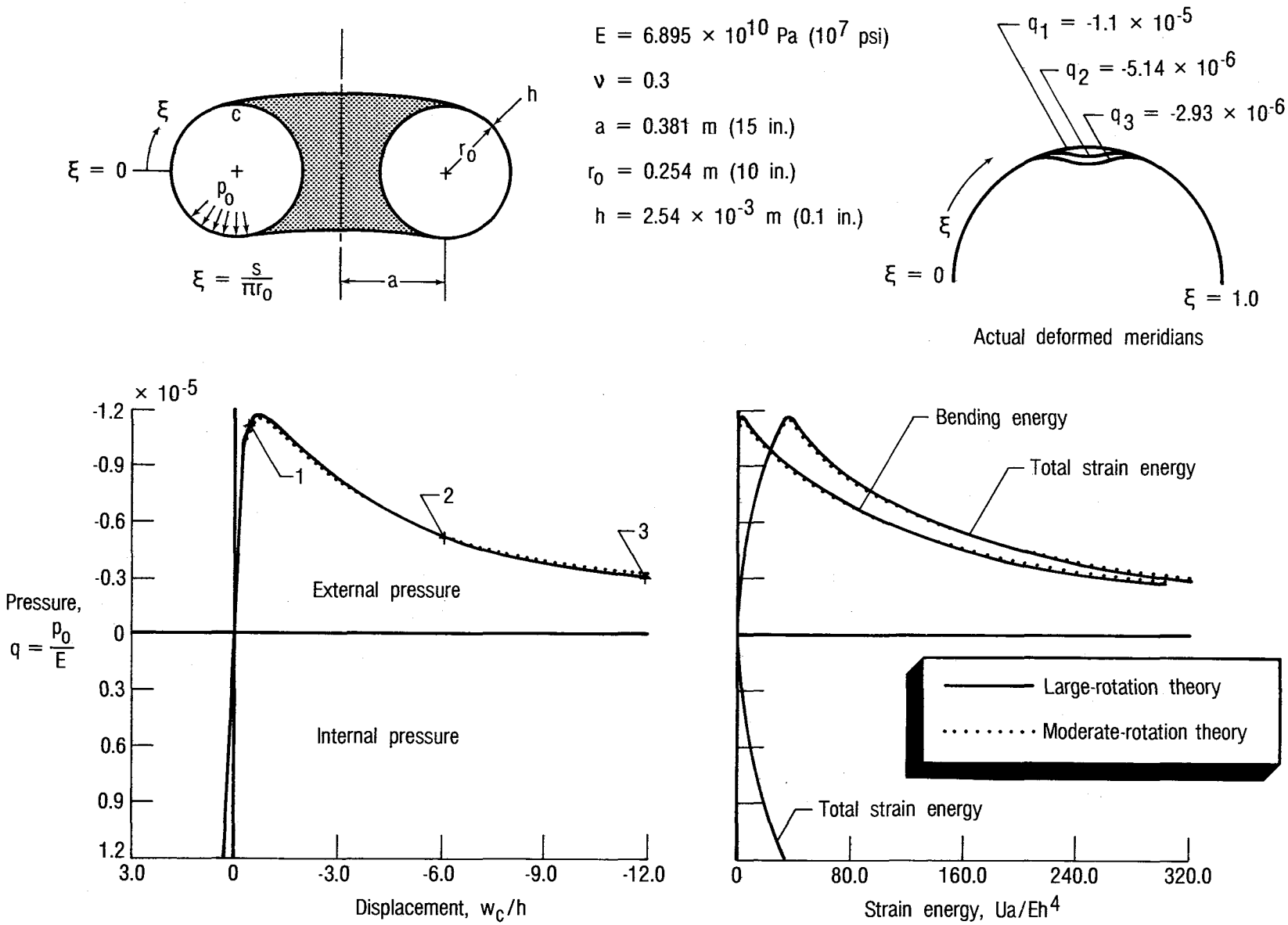

Figure 3.- Comparison of solutions obtained with large-rotation and moderate-rotation theories for circular toroidal shell subjected to uniform internal and external pressure loads.

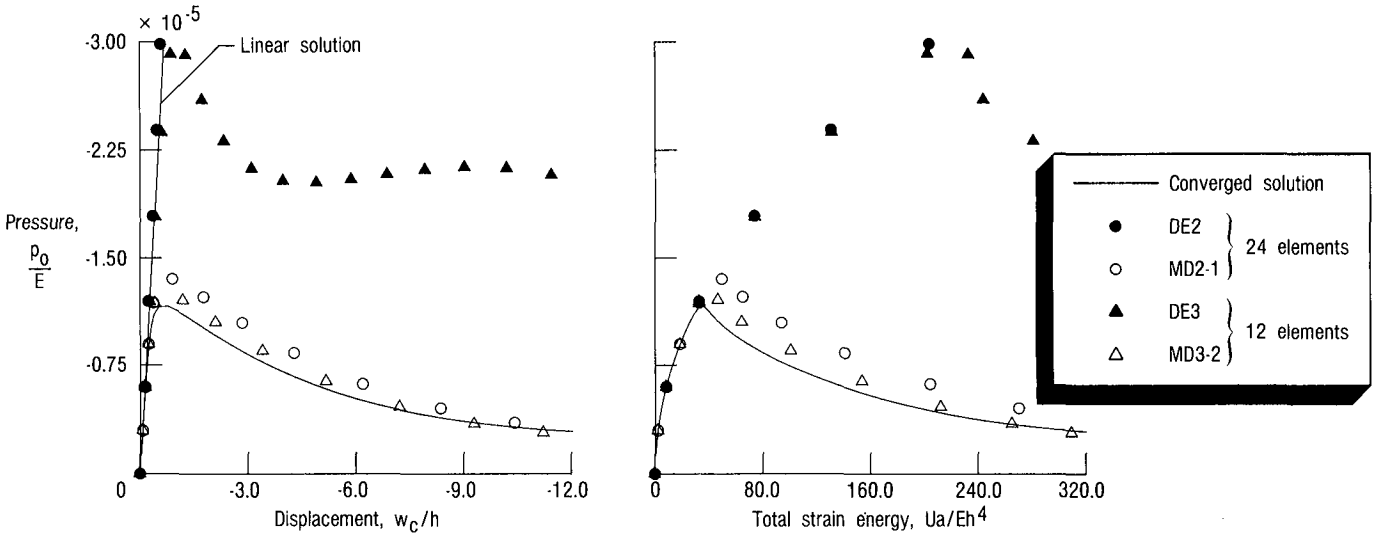

(a) Two- and three-node elements.

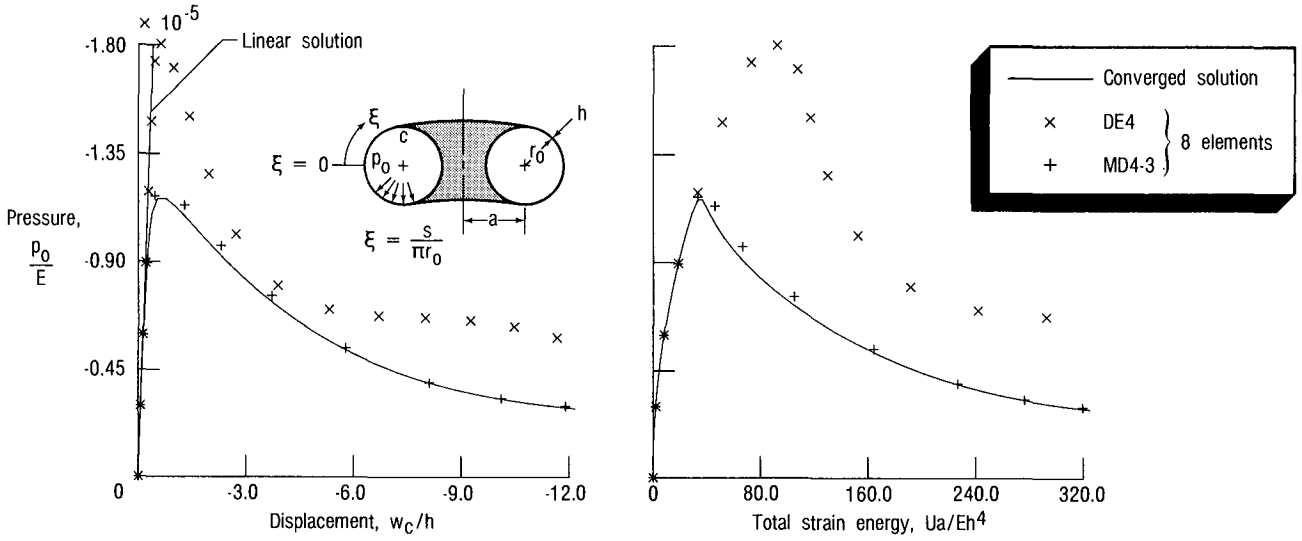

(b) Four-node elements.

Figure 4.- Accuracy of normal displacements and strain energies obtained with different displacement and mixed models for isotropic circular toroid subjected to uniform external pressure. (See fig. 3.)

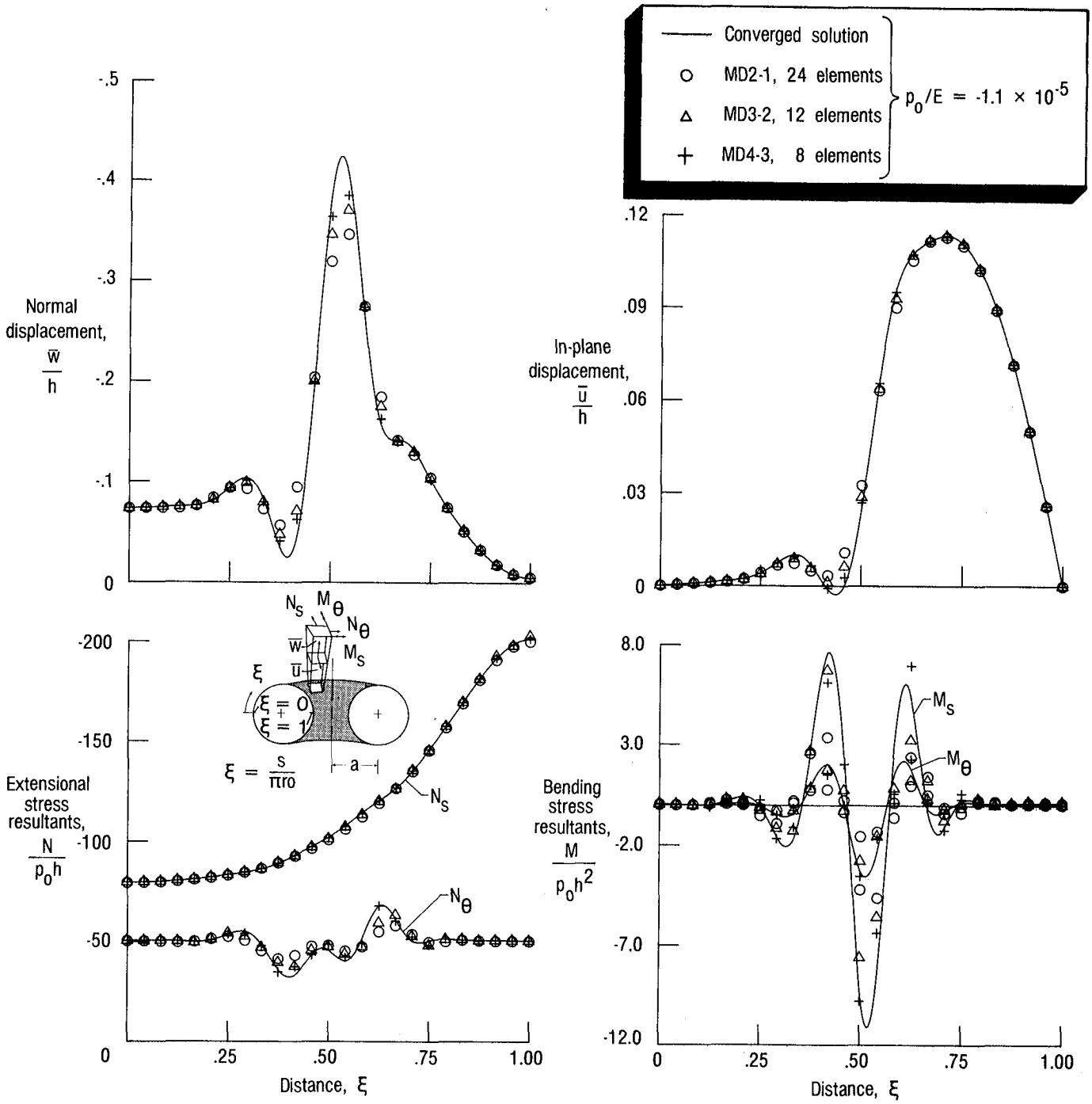

Figure 5.- Accuracy of displacements and stress resultants obtained with different mixed models for isotropic circular toroid subjected to uniform external pressure. (See fig. 3.)

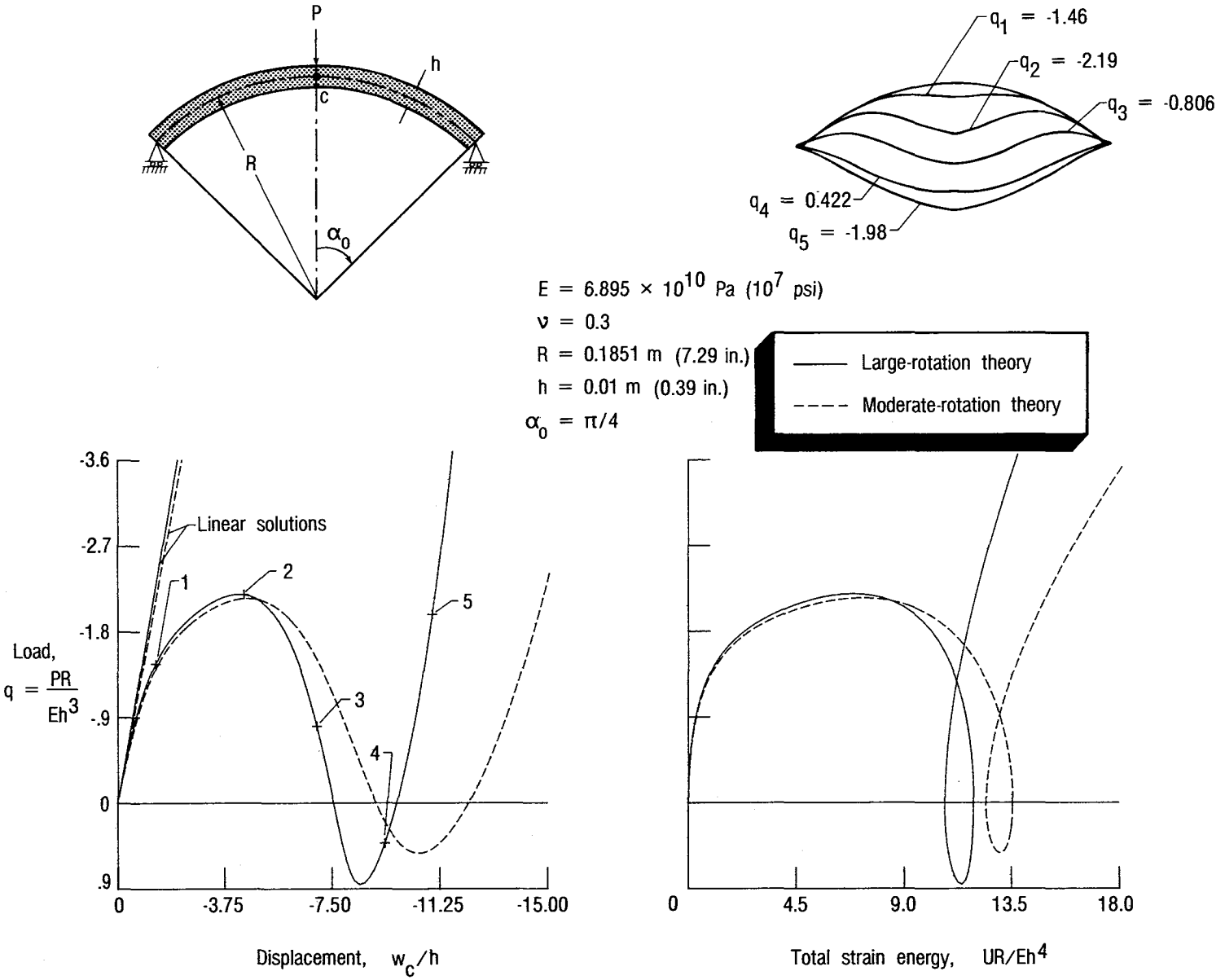

Figure 6.- Comparison of solutions obtained with large-rotation and moderate-rotation theories for isotropic spherical cap subjected to concentrated load at apex.

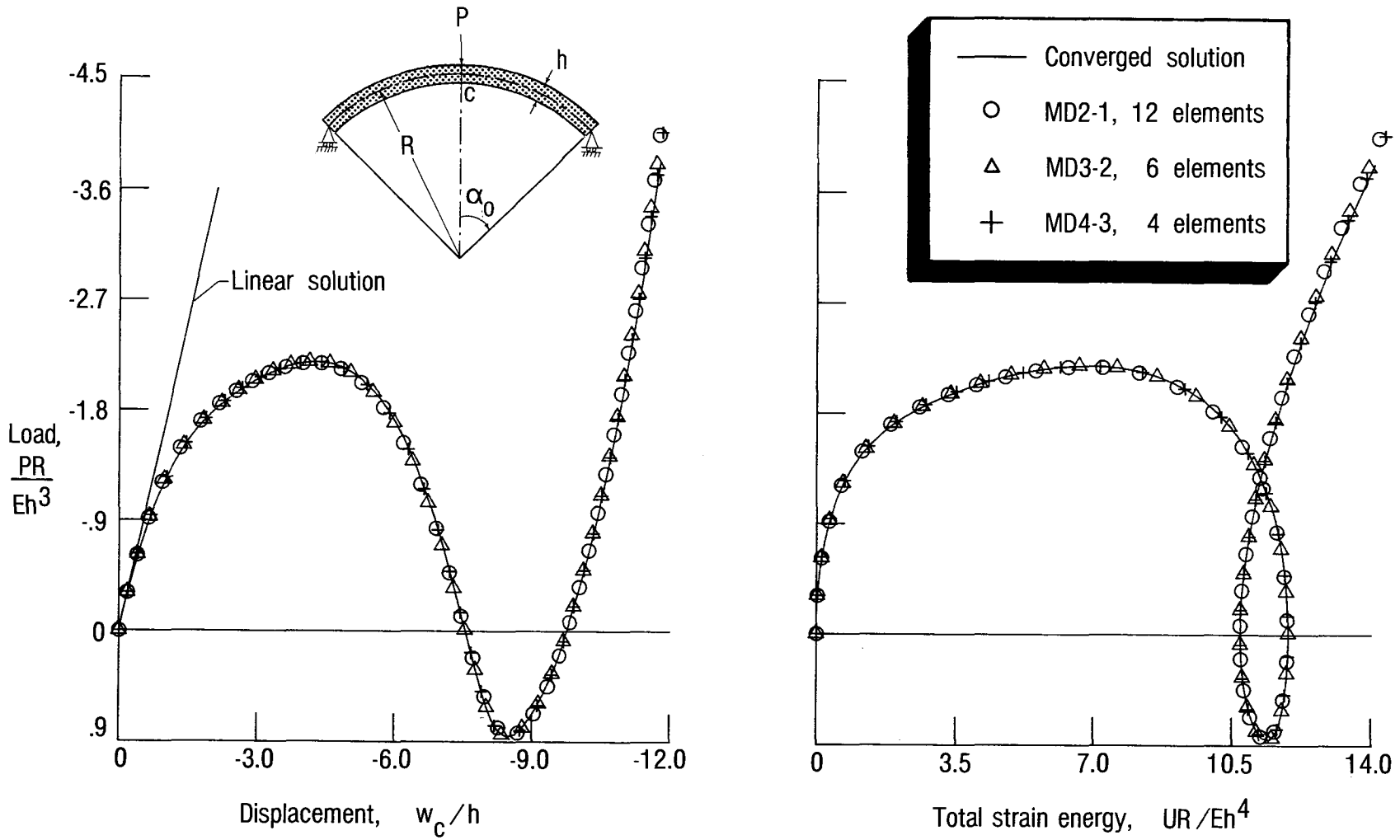

Figure 7.- Accuracy of solutions obtained with different mixed models at various load levels for isotropic spherical cap shown in figure 6.

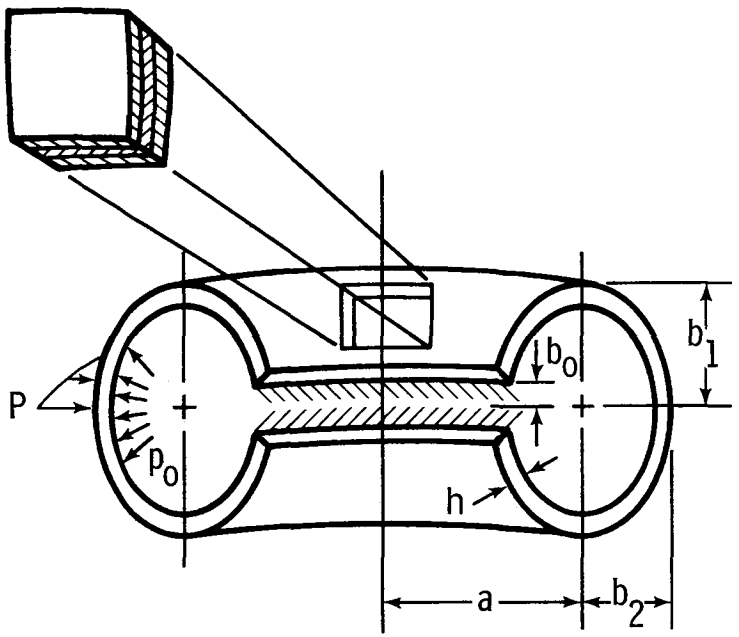

$E_L = 517 \times 10^6$ Pa (7.5×10^4 psi)

$E_T = 8.27 \times 10^6$ Pa (1.2×10^3 psi)

$G_{LT} = 3.10 \times 10^6$ Pa (450 psi)

$G_{TT} = 1.86 \times 10^6$ Pa (270 psi)

$\nu_{LT} = 0.4$

$h = 1.067 \times 10^{-2}$ m (0.42 in.)

$b_o = 5.08 \times 10^{-2}$ m (2.0 in.)

$b_1 = 6.223 \times 10^{-2}$ m (2.45 in.)

$b_2 = 5.385 \times 10^{-2}$ m (2.12 in.)

$a = 19.558 \times 10^{-2}$ m (7.70 in.)

Number of layers = 10

Fiber orientation: +45°/-45°/+45°/-45°/+45°/-45°/+45°/-45°/+45°/-45°

Figure 8.- Laminated orthotropic elliptical toroid shell used in present study.

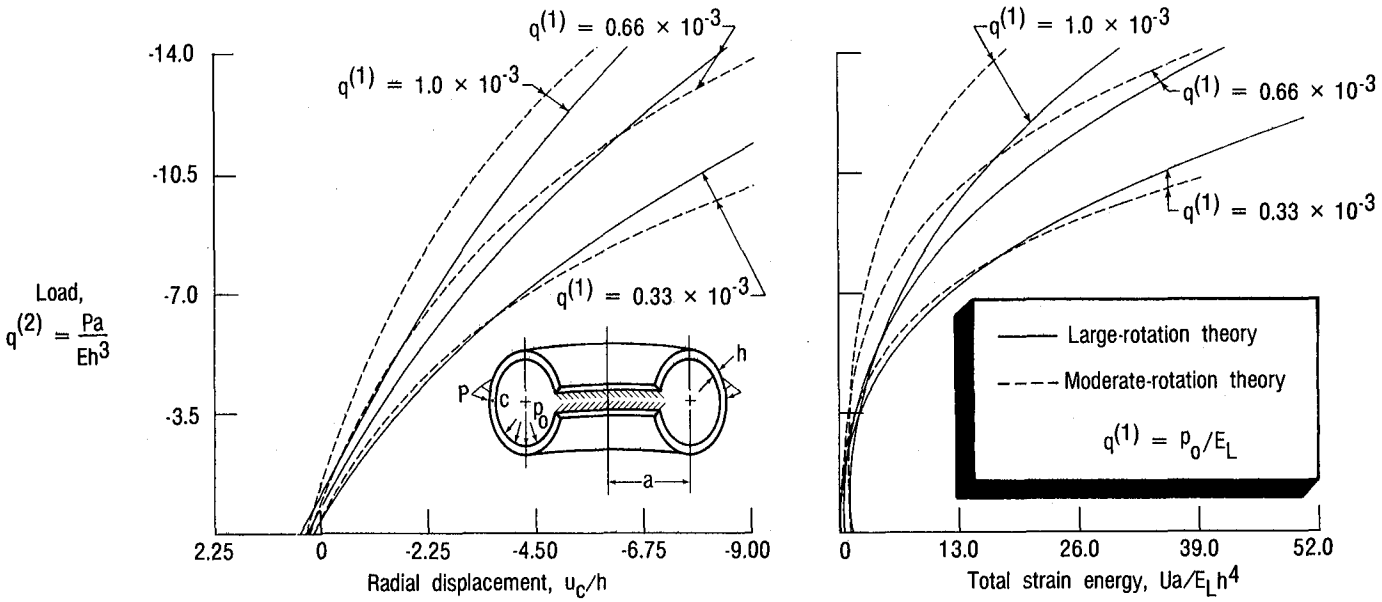

(a) Constant, directional pressure load.

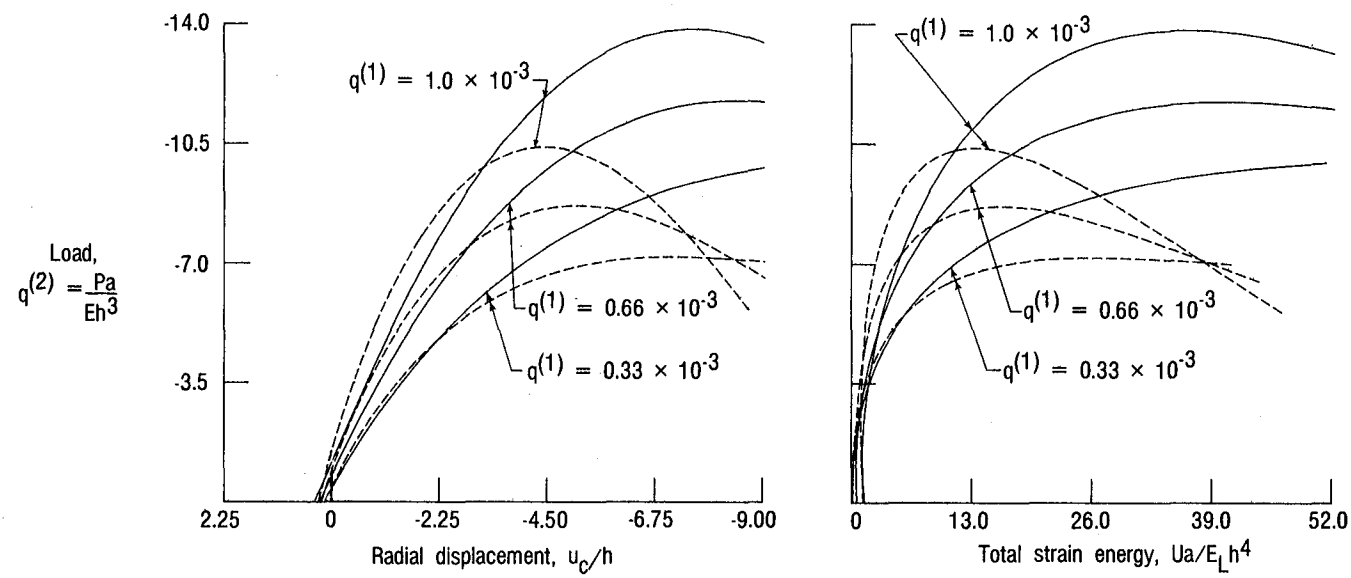

(b) Hydrostatic pressure load (live load).

Figure 9.- Comparison of solutions obtained with large-rotation and moderate-rotation theories for laminated, orthotropic elliptical toroid shell shown in figure 8.

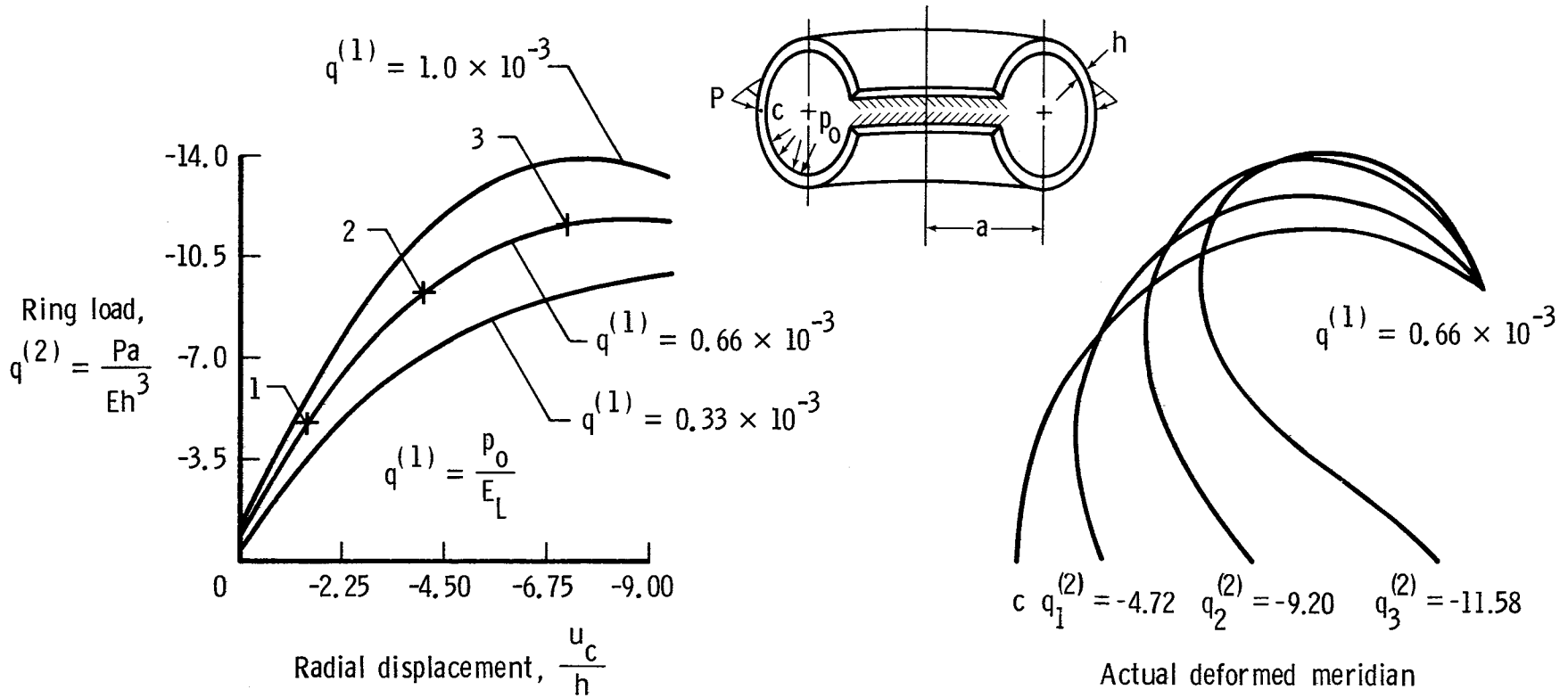

Figure 10.- Deformed configurations of laminated, orthotropic elliptical toroid shell subjected to combined internal hydrostatic pressure and external ring load. (See fig. 8.)

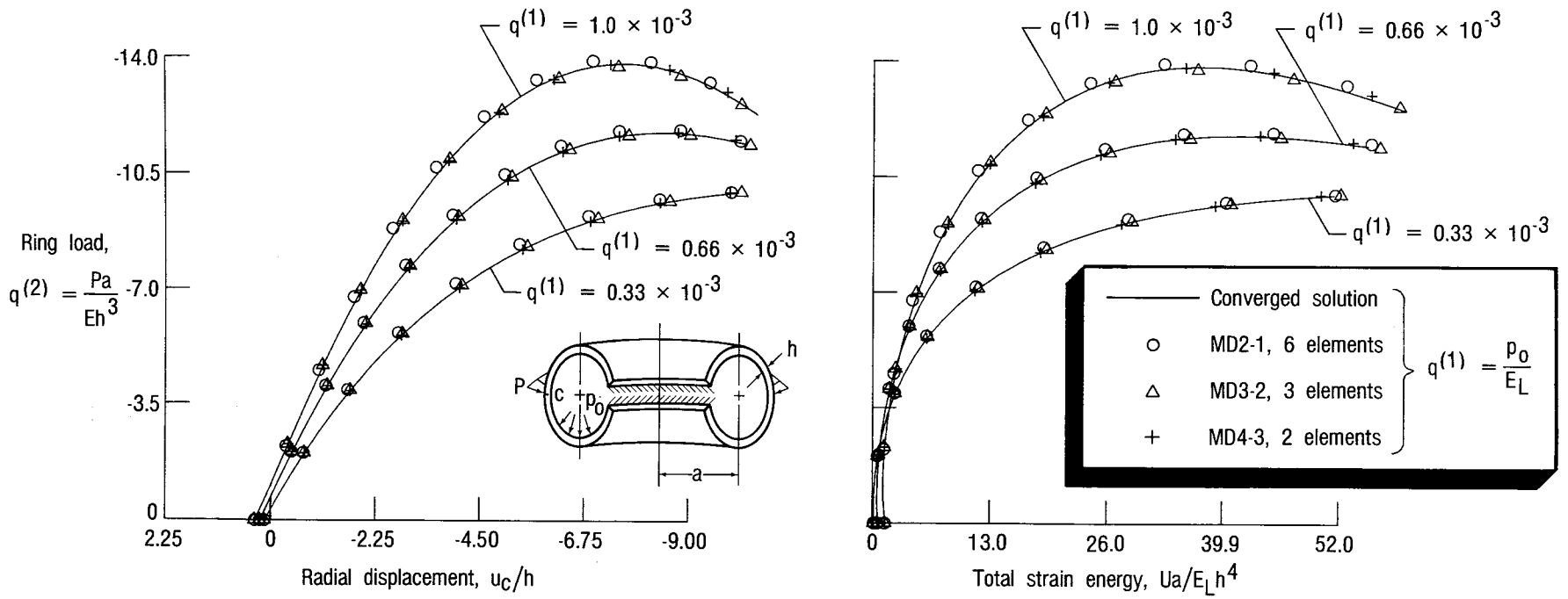

Figure 11.- Accuracy of radial displacements and strain energies obtained by using different mixed models for laminated, orthotropic elliptical toroid shell shown in figure 8.

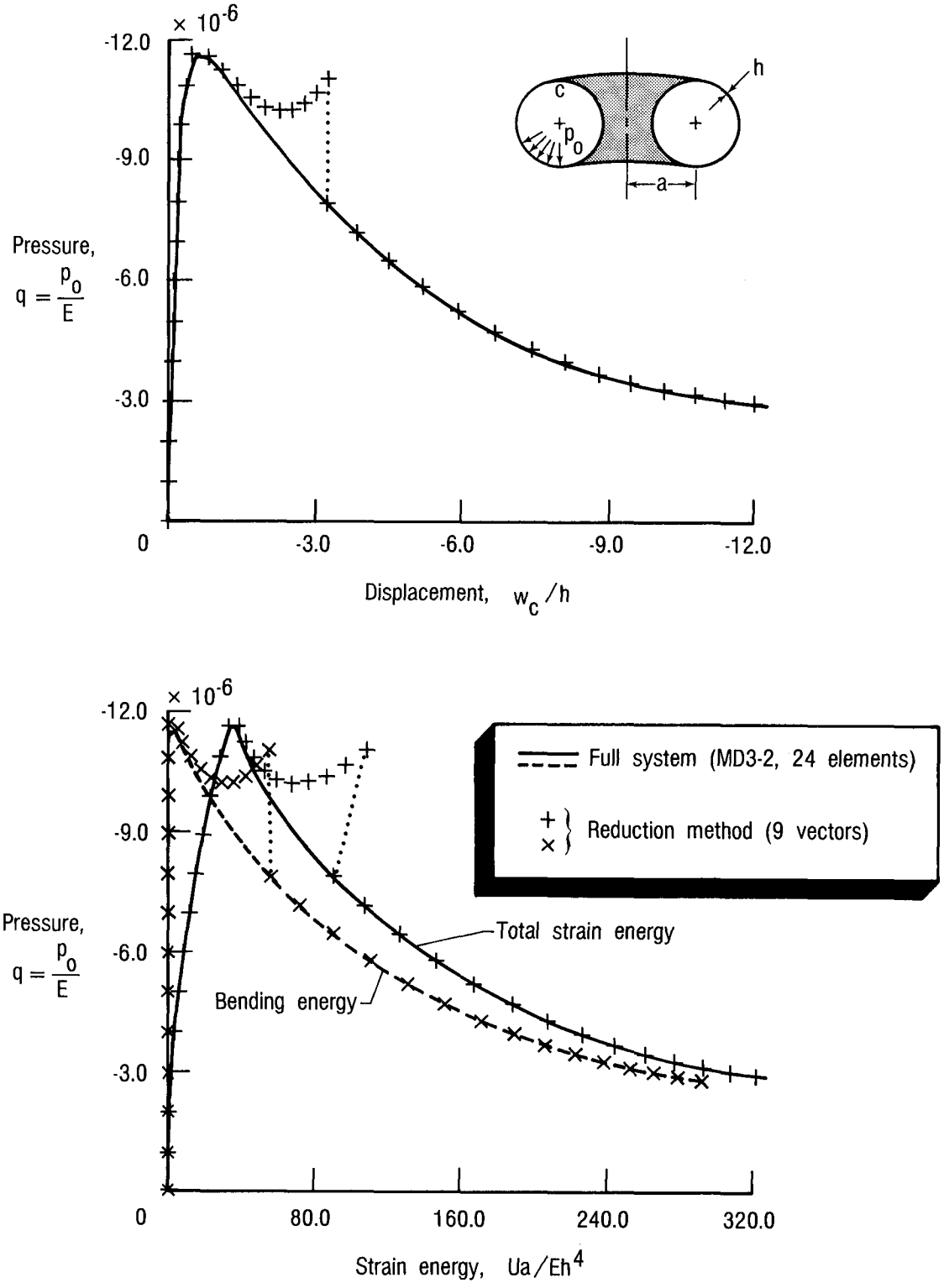

Figure 12.- Accuracy of solutions obtained with reduction method for isotropic circular toroid subjected to uniform pressure load. (See fig. 3.)

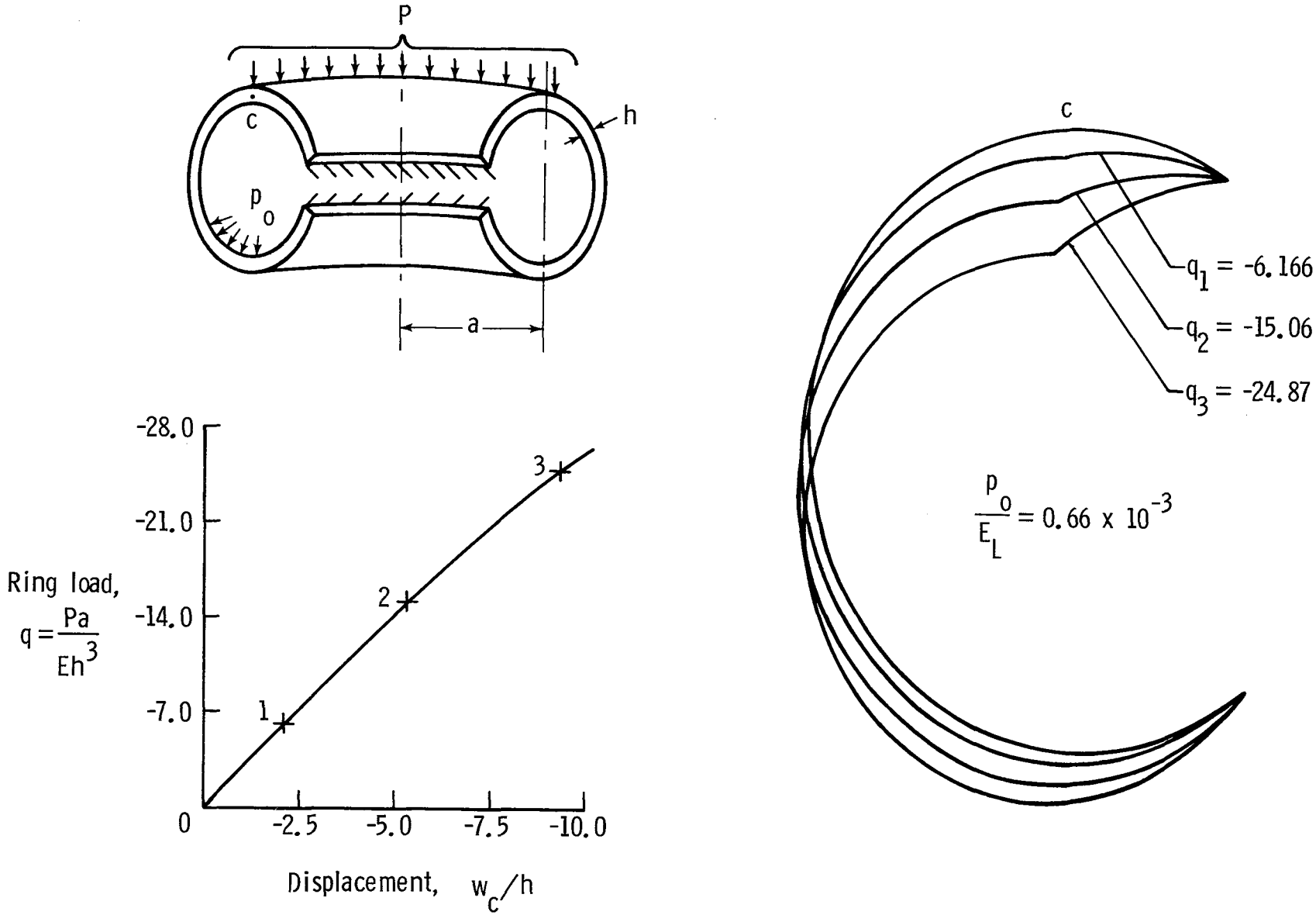

Figure 13.- Deformed configurations of laminated, anisotropic elliptical toroid shell subjected to combined asymmetric ring load and uniform hydrostatic pressure. (See fig. 8.)

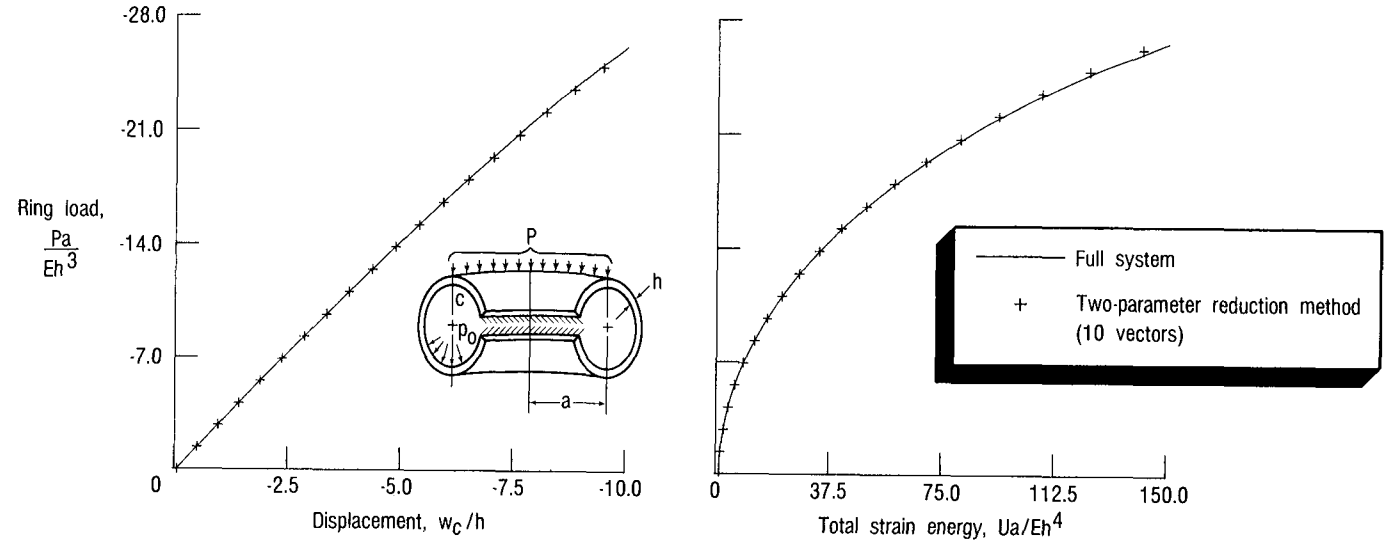

(a) Two-parameter reduction method (half model).

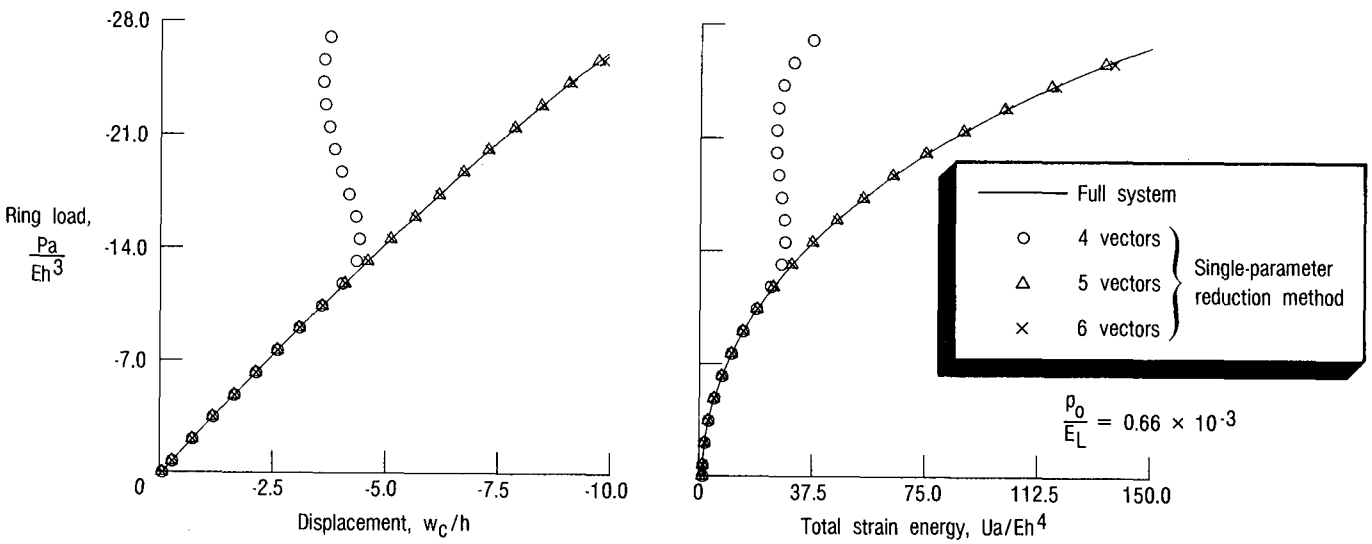

(b) Single-parameter reduction method (full model).

Figure 14.- Accuracy of two-parameter and single-parameter reduction methods for laminated, anisotropic elliptical toroid shell subjected to combined asymmetric ring load and uniform hydrostatic pressures. (See fig. 8.)

1. Report No.	2. Government Accession No.	3. Recipient's Catalog No.
NASA TP-2343		

4. Title and Subtitle	5. Report Date
MIXED MODELS AND REDUCTION TECHNIQUES FOR LARGE-ROTATION, NONLINEAR ANALYSIS OF SHELLS OF REVOLUTION WITH APPLICATION TO TIRES	October 1984
	6. Performing Organization Code 505-45-14-01
7. Author(s) Ahmed K. Noor, Carl M. Andersen, and John A. Tanner	8. Performing Organization Report No. L-15802
	10. Work Unit No.
9. Performing Organization Name and Address NASA Langley Research Center Hampton, VA 23665	11. Contract or Grant No.
	13. Type of Report and Period Covered Technical Paper
12. Sponsoring Agency Name and Address National Aeronautics and Space Administration Washington, DC 20546	14. Sponsoring Agency Code

15. Supplementary Notes

Ahmed K. Noor: The George Washington University, Joint Institute for Advancement of Flight Sciences, Langley Research Center, Hampton, Virginia.
Carl M. Andersen: The College of William and Mary, Williamsburg, Virginia; work performed under cooperative agreement NCCI-40.
John A. Tanner: Langley Research Center, Hampton, Virginia.

16. Abstract

An effective computational strategy is presented for the large-rotation, nonlinear axisymmetric analysis of shells of revolution. The three key elements of the computational strategy are: (1) use of mixed finite-element models with discontinuous stress resultants at the element interfaces; (2) substantial reduction in the total number of degrees of freedom through the use of a multiple-parameter reduction technique; and (3) reduction in the size of the analysis model through the decomposition of asymmetric loads into symmetric and antisymmetric components coupled with the use of the multiple-parameter reduction technique. The potential of the proposed computational strategy is discussed. Numerical results are presented to demonstrate the high accuracy of the mixed models developed and to show the potential of using the proposed computational strategy for the analysis of tires.

17. Key Words (Suggested by Author(s))		18. Distribution Statement
Axisymmetric shells	Nonlinear analysis	Unclassified - Unlimited
Finite elements	Reduction methods	
Large rotations	Symmetry concepts	
Mixed models	Tires	
Mixed variational principle	Taylor series expansions	Subject Category 39

19. Security Classif. (of this report)	20. Security Classif. (of this page)	21. No. of Pages	22. Price
Unclassified	Unclassified	56	A04

For sale by the National Technical Information Service, Springfield, Virginia 22161 NASA-Langley, 1984

National Aeronautics and
Space Administration

Washington, D.C.
20546

Official Business
Penalty for Private Use, $300

THIRD-CLASS BULK RATE

Postage and
National Aer
Space Administration
NASA-451

NASA

POSTMASTER: If Undeliverable (Section 158 Postal Manual) Do Not Return